AIMS Mathematics, 10(5): 11842–11879.
DOI: 10.3934/math.2025535
Received: 22 February 2025
Revised: 28 April 2025
Accepted: 06 May 2025
Published: 22 May 2025

http://www.aimspress.com/journal/Math

Research article

Advanced study of nonlinear partial differential equations in ion-acoustic and light pulses: solitons, chaos, and energy perspectives

Syed T. R. Rizvi[1], **M. A. Abdelkawy**[2], **Hanadi Zahed**[3,*] **and Aly R. Seadawy**[3,*]

[1] Department of Mathematics, COMSATS University Islamabad, Lahore Campus 54000, Pakistan
[2] Department of Mathematics and Statistics, College of Science, Imam Mohammad Ibn Saud Islamic University (IMSIU), Riyadh, Saudi Arabia
[3] Mathematics Department, Faculty of Science, Taibah University, Al-Madinah Al-Munawarah 41411, Saudi Arabia

* **Correspondence:** Email: aabdelalim@taibahu.edu.sa, hzahed@taibahu.edu.sa.

Abstract: The emphasis of this work is to apply the complete discriminant system (CDS) of a polynomial method (CDSPM) to obtain soliton solutions for the extended Korteweg–de Vries equation (EKdVE). The model of the KdV equation is suitable for describing water waves with shallow water, where the water depth is up to the wavelength. We explore exact and analytical solutions such as the hyperbolic function (HF), the Jacobian elliptic function (JEF), solitary wave (SW) solutions, and trigonometric solutions. Additionally, we apply bifurcation concept in qualitative model of the EKdVE. The procedure involves transforming the system into a planer dynamical system through a given transformation and examining bifurcation analysis. We also explore phase portraits which assist in determining the stability of the equilibrium point of the system. Additionally, chaotic behaviour (CB) exhibits the exponential divergence of the orbits, i.e., tiny differences in the initial condition result in widely divergent orbits over a time period. To explore the potential of CB, we insert a perturbed term to the dynamical system and proceed with caution to explore the model. From these, we obtain a linear combination resulting in a strong dynamic mathematical structure. Finally, we apply Jupyter as a machine learning program as well as Mathematica to graph some obtained solutions in various dimensions such as three-dimensional (3D) and two-dimensional (2D) plots by using some packages of PYTHON such as numpy, scipy.integrate, and matplotlib.pyplot. Additionally, we explore energy balance method (EBM), presenting approximate periodic solution of non-linear oscillatory systems. The method is based on principle of conservation of energy, total energy (sum of kinetic energy as well as potential energy) is conserved.

Keywords: soliton pulses; chaos analysis; qualitative analysis
Mathematics Subject Classification: 35J05, 35J10, 35K05, 35L05

1. Introduction

Recently, it has been increasingly exciting to solve exactly nonlinear partial differential equations (NLPDEs) with computational tools that make complicated algebraic calculations easier. In the field of soliton theory, exact solutions, especially solitary wave solutions to NLPDEs, play an important role in mathematical physics. Several areas of science use NLPDEs, such as fluid dynamics, plasma physics, chemical kinetics, quantum mechanics, ecological systems, biological models, nonlinear optics, electricity, ocean, and many others. It has been illustrated that NLPDEs are valuable tools for modelling nature's behaviors in many areas of science and engineering [1, 2]. Thus, it is important that one should be up to date with new analytical and numerical methods for modeling any physical or natural problem [3–5]. Several authors have studied the fractional nonlinear model [6–8]. The Korteweg-de Vries (KdV) equation is an established PDE which became popular over the 50 years since it was established due to its ability to model many natural and physical phenomena in many fields of science [9, 10]. It models extended one-dimensional structures' evolution (solitary waves and cnoidal waves) in the ocean, water tanks, various plasma models, and nonlinear optics [11, 12]. It can also be applied to model inner waves in the sea with a number of density layers, crystal lattice acoustic waves, and plasma ion-acoustic wave models [13–15]. In fluid dynamics, the KdV equation plays an important role, since it models wave propagation in dispersive and nonlinear media [16, 17]. Due to its way of expression, it serves as a suitable investigation application to study many fluids phenomena like shallow water waves, soliton dynamic, and nonlinear waves interactions [18, 19]. Using the help of the perturbation reduction method, Neirameh et al. proposed the extended KdV equation by providing a double-layered structure in the available plasma model [20–22]. Now, we propose the extended KdV equation by employing fractional derivatives which are given as follows [23]:

$$((1-f)E_1 + fF_1\sigma - \frac{1}{\lambda^2})\psi_2 = (\frac{3}{2\lambda^4} - ((1-f)E_2) + fF_2\sigma^2)(\psi_1)^2, \tag{I}$$

where

$$E_1 = \frac{\kappa_c - \frac{1}{2}}{\kappa_c - \frac{3}{2}},\ \ F_1 = \frac{\kappa_h - \frac{1}{2}}{\kappa_h - \frac{3}{2}}, E_2 = \frac{(\kappa_c - \frac{1}{2})(\kappa_c + \frac{1}{2})}{2(\kappa_c - \frac{3}{2})^2}, \qquad F_2 = \frac{(\kappa_h - \frac{1}{2})(\kappa_h + \frac{1}{2})}{2(\kappa_h - \frac{3}{2})^2}, \tag{II}$$

$$\frac{\partial n_1}{\partial \sigma} - \lambda\frac{\partial n_3}{\partial \xi} + \frac{n_2u_1}{\partial \xi} + \frac{n_1u_2}{\partial \xi} + \frac{u_3}{\partial \xi} = 0, \tag{III}$$

$$\frac{\partial u_1}{\partial \sigma} - \lambda\frac{\partial u_1}{\partial \xi} + u_1\frac{u_2}{\partial \xi} - \lambda\frac{u_3}{\partial \xi} + \frac{\psi_3}{\partial \xi} = 0, \tag{IV}$$

$$\frac{\partial^2\psi_1}{\partial\xi^2} + (\frac{3}{2\lambda^4} - (1-f)E_2 + fF_2\sigma^2)(\psi_1)^2 = \frac{1}{\lambda^2}\psi_3 + 2((1-f)E_2) + fF_2\sigma^2(\psi_1\psi_2) + (E_3(1-f) + f\sigma^3F_3)\psi^3 - n_3, \tag{V}$$

$$\frac{\partial\psi_1}{\partial\sigma} + \frac{\lambda^3}{2}(\frac{3}{2\lambda^4} - (1-f)E_2 + fF_2\sigma^2)(\frac{\psi_1}{\partial\xi})^2 + \frac{\lambda^3}{2}(\frac{5}{2\lambda^6} - 2((1-f)E_3) + fF_3\sigma^3(\frac{\partial\psi_1}{\partial\xi})^3)\frac{\lambda^3}{2}\frac{\partial^3\psi_1}{\partial\xi^3} = 0, \tag{VI}$$

$$\mu = \sqrt{\frac{1}{E_1(1-f) + F_1f\sigma}}, \qquad \tau = \frac{T_c}{T_h}, \qquad f = \frac{n_{h0}}{n_{i0}}, \tag{1.1}$$

$$1-f=\frac{n_{c0}}{n_{i0}}, \qquad n_{i0}=n_{c0}+n_{h0},$$
$$E_3=\frac{(\kappa_c-\frac{1}{2})(\kappa_c+\frac{1}{2})(\kappa_c+\frac{3}{2})}{6(\kappa_c-\frac{3}{2})^3},$$
$$F_3=\frac{(\kappa_h-\frac{1}{2})(\kappa_h+\frac{1}{2})(\kappa_h+\frac{3}{2})}{6(\kappa_h-\frac{3}{2})^3}.$$

Our main goal is to study the following equation:

$$D_\sigma^\alpha\psi_1+\frac{\mu^3}{2}[\frac{3}{2\mu^4}-(E_2(1-f)+F_2f\tau^2)]D_\xi^{2\alpha}\psi_1+\frac{\mu^3}{2}(\frac{5}{2\mu^6}-E_3(1-f)-f\tau^3F_3)(D_\xi^\alpha\psi_1)^3+\frac{\mu^3}{2}D_\xi^{3\alpha}\psi_1=0, \tag{1.2}$$

where $D_\sigma^\alpha\psi_1$ denotes the α order derivative of ψ_1 with respect to σ and σ denotes the time derivative. Similarly, $D_\xi^{2\alpha}\psi_1$ denotes the 2αth order derivative of ψ_1 with respect to ξ, which represents the spatial derivative.

Here, we treat the plasma with cold ions and two sets of electrons of different types: cold electrons and hot electrons. Thus, the temperatures of hot electrons and cold electrons are given by T_c and T_h. The ion density, density of cold electrons, density of hot electrons are denoted by n, n_c, and n_h. Moreover, κ_c and κ_h represent real values that are the spectral index measuring deviations from Maxwellian equilibrium for cold electrons and hot electrons, respectively. The governing nonlinear evolution equation modeling electrostatic wave dynamics in ultra-dense quantum plasmas with fractional effects. Its significance lies in, bridging physical realism (quantum + relativistic effects) with mathematical solvability, enabling the discovery of new optical soliton and wave packet solutions, and generalizing classical models like the KdV equation to modern, high-energy, and astrophysical plasma systems.

Our primary goal is to examine Eq (1.2) to find solitons and wave structures by applying the complete discriminant system for polynomials method (CDSPM) [24–26]. The proposed method has various merits over earlier methods because it describes the findings in a general, explicit way with rational, trigonometric, hyperbolic (HF), and Jacobian elliptic (JEF) function solutions. We also demonstrate our solutions' dynamical behaviors by employing bifurcation and chaotic behavior (CB) [27–29]. For a better understanding of bifurcation analysis, sensitivity to initial conditions, and the basics of chaotic dynamics, scientists have usually studied two-dimensional (2D) chaotic systems. Bifurcation theory studies and chaotic behavior have revealed astonishing attributes for dynamical systems in the last decade. To obtain an insight to the complex behaviors exhibited by the system, bifurcation study is also performed by using well established theory of planar dynamical systems [30–32]. Bifurcation demonstrates how dynamical systems behave if the values of certain parameters are varied [33–35]. The development of chaos theory and study of the complex behavior of the nonlinear waves play central role in differential equation (DE). To achieve this, a dynamical system is analyzed and amplified by an external term. Studying chaos is important in the 21th century and it is focused on time analysis, Poincare maps, and phase portraits. Some vital papers in the massive domain of soliton solutions and bifurcation are available in the literature. These papers examine the complicated dynamics of nonlinear systems, providing insight to the intriguing behavior of solitons and the bifurcation mechanisms controlling them. Research into such systems not only develops the theoretical aspects of chaos theory but also is applied in secure communication, random number

generation, and some fields where pseudorandomism and unpredictability are required. Afzal et al. [36] generated multi-solitons and explored chaos and the bifurcation of waves in shallow water. Lie and Huang applied bifurcation and chaos theory to study the conformable Fokas-Lenells model [37]. Zhang et al. investigated bifurcation using the modified Fitz-Hugh-Nagumo neuron model and found new solutions [38]. As far as we can understand, no earlier study has considered bifurcation and CB of the extended KdV equation (EKdVE).

In this paper, we have explored the extended KdV equation (EKdVE) equation for different types of solitary wave solutions such as bell-shaped, kink-shape, straddled solitons and other solitary wave solutions by using an integration approach called the CDSPM. We also examine the qualitative behavior of our governing model with chaotic behavior and sensitivity. We also make use of the energy balance approach to provide the energy analysis for our governing model. This paper includes a variety of new and innovative solutions. This investigation offers tools and insight that can assist in solving every-day world problems in systems governed by non-linear wave equations that could enhance technological solutions in energy transmission, communication networks, fluid controlling systems, etc.

2. CDSPM analysis

Our investigation of the CDSPM, which has been implemented to solve many nonlinear models, involves bifurcation study and a brief discussion on determining the solitons solutions of NLPDEs [27]. Let us first consider the following NLPDE, see Table 1.

$$R(\Phi, \Phi_t, \Phi_{xx}, ...) = 0. \tag{2.1}$$

Table 1. Python libraries for evaluating and graphing the solution.

Library	Usage
Pandas and numpy	Data analysis
matplotlib.pyplot as plt	Graphical and plotting interfaces
scipy.integrate	Offers a platform for conducting multiple approaches of numerical integration

Step 1. Utilize the transformation $\Phi(x,t) = \Phi(\varphi)$ & $\varphi = \tau x - \ell t$, to obtain an ordinary differential equation (ODE):

$$R(\Phi, \Phi^{'}, \Phi^{''}, ...) = 0, \tag{2.2}$$

where the prime in the $\Phi^{'}$ denotes the first derivative and the double prime in $\Phi^{''}$ shows the second derivative and so on.

Step 2. The ODE mentioned above fulfills the following equation:

$$(\Phi')^2 = \Phi^4 + a_2\Phi^2 + a_1\Phi + a_0. \tag{2.3}$$

This equation's integral form is:

$$\pm(\varphi - \varphi_0) = \int \frac{d\Phi}{\sqrt{\Phi^4 + a_2\Phi^2 + a_1\Phi + a_0}}. \tag{2.4}$$

Step 3. Let $h(\Phi) = \Phi^4 + a_2\Phi^2 + a_1\Phi + a_0$. According to the fourth-order polynomial CDS:

$$O_1 = 4, \quad O_2 = -f_2, \quad O_3 = -2f_2^3 + 8f_2f_0 - 9f_1^2, \tag{2.5}$$
$$O_4 = -f_2^3f_1^2 + 4f_2^2f_0 + 36f_2f_1^2f_0 - 32f_2^2f_0 - \frac{-27}{4}f_1^4 + 63f_0^3,$$
$$H_2 = 9f_2^2 - 32f_2f_0.$$

It can be determined what type of classification the equation's solutions are:
Step 4. The dynamic system that conforms to Eq (2.4), which is presented below:

$$\begin{cases} \Phi' = P(\varphi), \\ P' = 4\Phi^3 + 2a_2\Phi + a_1, \end{cases} \tag{2.6}$$

and the hamiltonian of the system are as follow:

$$H(\Phi, P) = \frac{P^2}{2} + \frac{1}{2}(\Phi^4 + a_2\Phi^2 + a_1\Phi + a_0). \tag{2.7}$$

Now, by using hamiltonian we get the potential energy that is shown below:

$$U(\Phi) = \Phi^4 + a_2\Phi^2 + a_1\Phi + a_0. \tag{2.8}$$

Thus, to identify dynamics features, we can get the roots of $U'(\Phi)$. Next, we talk of four kinds of cases with the shape of $U'(L)$ that inform us regarding equilibrium points and bifurcation.

3. Mathematical model

In this article, we obtain bifurcation and optical solitons of Eq (1.2) by CDSPM. We consider $\varphi = (\frac{1}{\alpha})\xi^\alpha - V(\frac{1}{\alpha})\sigma^\alpha$, So,

$$-V\psi_1 + \frac{\mu^3}{2}[\frac{3}{2\mu^4} - (E_2(1-f) + F_2f\tau^2)]\psi_1^2 + \frac{\mu^3}{2}(\frac{5}{2\mu^6} - E_3(1-f) - f\tau^3F_3)\psi_1^3 + \frac{\mu^3}{2}\psi_1'' = 0. \tag{3.1}$$

Dividing Eq (3.1) by $\frac{2}{\mu^3}$, then, we get,

$$-\frac{2V}{\mu^3}\psi_1 + [\frac{3}{2\mu^4} - (E_2(1-f) + F_2f\tau^2)]\psi_1^2 + (\frac{5}{2\mu^6} - E_3(1-f) - f\tau^3F_3)\psi_1^3 + \psi_1'' = 0. \tag{3.2}$$

Let $M = (\frac{5}{2\mu^6} - E_3(1-f) - f\tau^3F_3)$, $N = [\frac{3}{2\mu^4} - (E_2(1-f) + F_2f\tau^2)]$, and $Q = -\frac{2V}{\mu^3}$, then, Eq (3.2) becomes:

$$\psi_1'' + M\psi_1^3 + N\psi_1^2 + Q\psi_1 = 0. \tag{3.3}$$

After multiplying Eq (3.3) by $2\psi_1' d\varphi$ to get the integration result,

$$(\psi_1')^2 + \frac{M}{2}\psi_1^4 + \frac{2N}{3}\psi_1^3 + Q\psi_1^2 + 2A = 0, \tag{3.4}$$

where A is an integration constant.

Now, Eq (3.4) becomes

$$(\psi_1')^2 = -\phi_3(\psi_1^4 + \phi_2\psi_1^3 + \phi_1\psi_1^2 + \phi_0), \tag{3.5}$$

where

$$\phi_3 = \frac{M}{2}, \quad \phi_2 = \frac{4N}{3M}, \quad \phi_1 = \frac{2Q}{M}, \quad \phi_0 = \frac{4A}{M}. \tag{3.6}$$

To get the classification of solutions, we can consider the following substitution:

$$\psi_1 = L + \frac{\phi_2}{4}, \tag{3.7}$$

then, we get

$$(L')^2 = -\phi_3(L^4 + f_2L^2 + f_1L + f_0), \tag{3.8}$$

where

$$f_2 = \frac{-7\phi_2^2 + 16\phi_1}{16}, \quad f_1 = \frac{\phi_2(\phi_2 - 4\phi_1)}{8}, \quad f_0 = \frac{-2\phi_2^4 + 64\phi_2^2\phi_1 + 256\phi_0}{256}. \tag{3.9}$$

Now, Eq (3.8) tackles both the $\phi_3 < 0$ and $\phi_3 > 0$ cases. Integral form of Eq (3.8) is

$$\int \frac{df}{\sqrt{L^4 + f_2L^2 + f_1L + f_0}} = \pm\sqrt{-\phi_3}(\varphi - \varphi_0), \tag{3.10}$$

where φ_0 is an integration constant. Let $R(L) = L^4 + f_2L^2 + f_1L + f_0$ and CDS as follows:

$$\begin{gathered} O_1 = 4, \;\; O_2 = -f_2, \;\; O_3 = -2f_2^3 + 8f_2f_0 - 9f_1^2, \\ O_4 = -f_2^3f_1^2 + 4f_2^2f_0 + 36f_2f_1^2f_0 - 32f_2^2f_0 - \frac{-27}{4}f_1^4 + 63f_0^3, \\ H_2 = 9f_2^2 - 32f_2f_0. \end{gathered} \tag{3.11}$$

H_2 is the discrimination of $\Delta_2(R)$. The dynamic system displayed below clearly satisfies Eq (18),

$$\begin{cases} L' = P(\varphi), \\ P' = -\phi_3(4L^3 + 2f_2L + f_1). \end{cases} \tag{3.12}$$

The Hamiltonian of the system is stated as follows:

$$H(L, P) = \frac{P^2}{2} + \frac{(-\phi_3)}{2}(L^4 + f_2L^2 + f_1L + f_0). \tag{3.13}$$

Thus, the potential energy is given by

$$U(L) = -\phi_3(L^4 + f_2L^2 + f_1L + f_0). \tag{3.14}$$

3.1. Qualitative-analysis

To examine the dynamic characteristics of Eq (3.8), it is required to determine the roots of $U'(L)$ [27]

$$U'(L) = -2\phi_3(L^3 + g_1L + g_0), \tag{3.15}$$

where $g_1 = \frac{f_2}{2}$ and $g_0 = \frac{f_1}{4}$. Thus, we have Jacobian,

$$J(L,P) = \begin{vmatrix} 0 & 1 \\ 2\phi_3(3L^2 + g_1) & 0 \end{vmatrix} = -2N(3L^2 + g_1). \tag{3.16}$$

Therefore, it is simple to demonstrate that the eigenvalues at the specific point $(L, 0)$ are,

$$\lambda \pm (L, 0) = \pm\sqrt{2\phi_3(3L^2 + g_1)}. \tag{3.17}$$

Thus, the saddle point exists at $(L, 0)$ if $J(L, P) < 0$, there will exist a cuspidal point if $J(L, P) = 0$, and a centre if $J(L, P) > 0$. Since, CDS is represented by

$$\Delta = -(\frac{g_0^2}{4} + \frac{g_1^3}{27}). \tag{3.18}$$

The CDSPM can be used to explore three scenarios of the form $U'(L)$.

Case 1. $\Delta = 0$ & $g_1 < 0$,

$$U'(L) = -\phi_3(L - i)^2(L - j), (2i + j = 0). \tag{3.19}$$

There are two equilibrium points for the dynamic system: $(i, 0)$, which is the cuspidal point, and $(j, 0)$, which is the saddle point. Taking, for instance, $g_1 = -3$ and $g_0 = 2$ yields $i = 1$ and $j = -2$. Phase picture under this situation is illustrated in Figure 1.

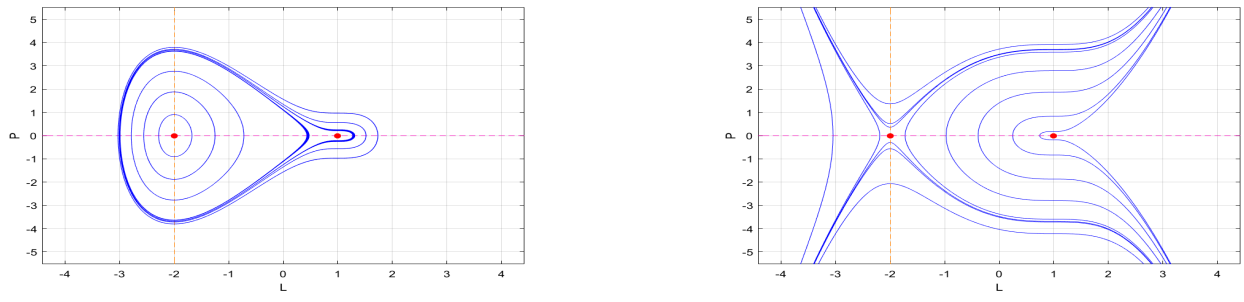

(a) **(b)**

Figure 1. The system (3.12) exhibits bifurcation portrait in Case 1: (a) $\phi_3 = \frac{1}{2}$, (b) $\phi_3 = -\frac{1}{2}$.

Case 2. $\Delta = 0$ & $g_1 = 0$,

$$U'(L) = -\phi_3 L^3. \tag{3.20}$$

It possesses a single equilibrium point, denoted by $(0, 0)$, that is referred to as the cuspidal point. Phase portrait under bifurcation conditions $\phi_3 = \pm\frac{1}{2}$ and $g_0 = 0$ is illustrated in Figure 2.

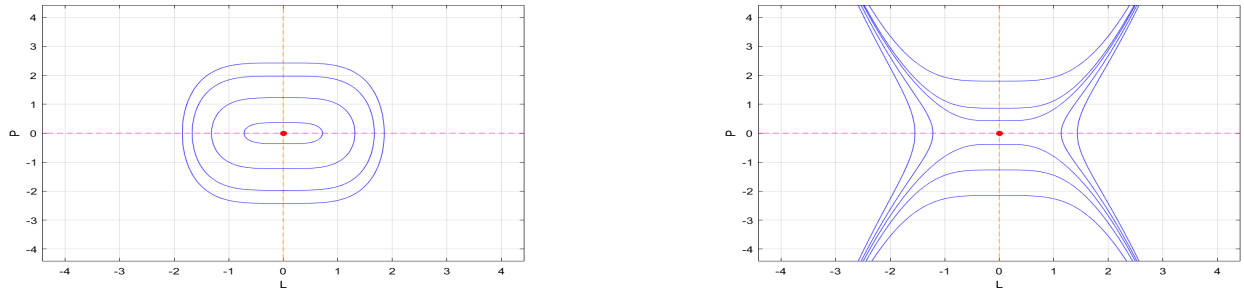

(a) **(b)**

Figure 2. For Eq (3.12), bifurcation portrait for Case 2: (a) $\phi_3 = \frac{1}{2}$, (b) $\phi_3 = -\frac{1}{2}$.

Case 3. $\Delta > 0$ & $g_1 < 0$,

$$U'(L) = -\phi_3(L - i)(L - j)(L - k), (i + j + k = 0). \tag{3.21}$$

The system has three equilibrium points: $(i, 0)$, $(j, 0)$, and $(k, 0)$ in the event that $i > j > k$. Specifically, we have $i = 1$, $j = 0$, and $k = -1$ by substituting values $g_1 = -1, g_0 = 0$, and $\phi_3 = \frac{1}{2}$. The center points are $(i, 0)$ and $(k, 0)$, with $(j, 0)$ being a saddle point. On the contrary, with $\phi_3 = -\frac{1}{2}$, $(j, 0)$ is now a center point, with $(i, 0)$, and $(k, 0)$ being saddle, see Figure 3.

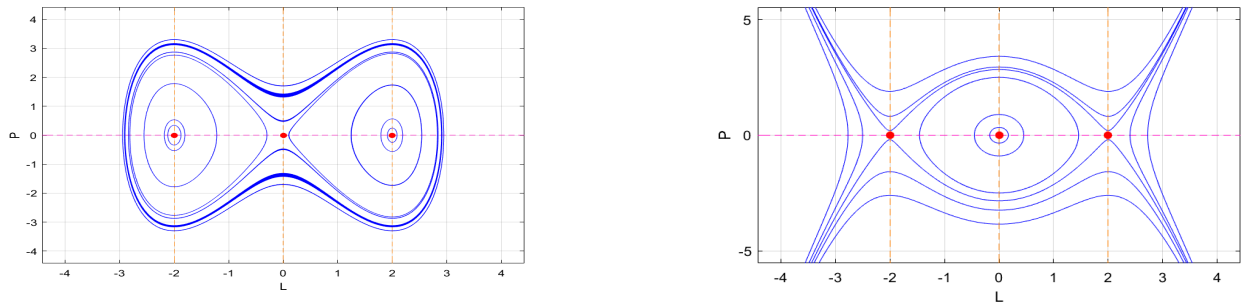

(a) **(b)**

Figure 3. For Eq (3.12), bifurcation portrait for Case 3: (a) $\phi_3 = \frac{1}{2}$, (b) $\phi_3 = -\frac{1}{2}$.

Case 4: $\Delta < 0$

$$U'(L) = -\phi_3(L - k)[(L - l)^2 + i^2], (k + 2l = 0). \tag{3.22}$$

There exists an equilibrium point in the dynamic system at $(0, 0)$. When we take values for $g_0 = 0$, $g_1 = 1$, and $\phi_3 = \frac{1}{2}$, then, it assumes the nature of a saddle. On taking $\phi_3 = -\frac{1}{2}$, it becomes a

center. Global phase image of relevance to perform bifurcation analysis is depicted in Figure 4. The results show that changing any of the parameters, particularly equilibrium points, drastically varies the dynamic attributes. It is easier to study many types of equilibrium points and bifurcations under the CDSPM.

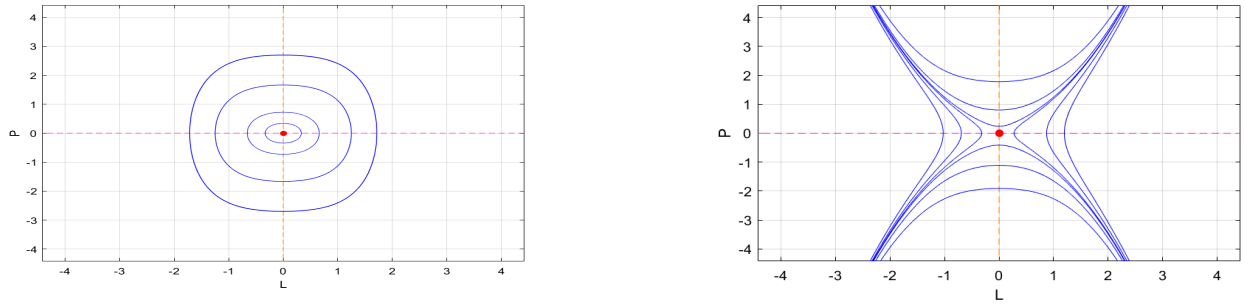

(a) **(b)**

Figure 4. For Eq (3.12), bifurcation portrait for Case 4: (a) $\phi_3 = \frac{1}{2}$, (b) $\phi_3 = -\frac{1}{2}$.

3.2. Exact-solutions

CDSPM is also utilized to find the exact solution with following cases:

Case 1. $O_2 < 0$, $O_3 = 0$, and $O_4 = 0$. Then, we have

$$R(L) = ((L - \theta)^2 + m)^2. \tag{3.23}$$

For $m > 0$ and $\phi_3 < 0$, we use Eq (18) to obtain:

$$L = \theta + \vartheta \tan(\vartheta \sqrt{-\phi_3}(\varphi - \varphi_0)). \tag{3.24}$$

Therefore, we get the solution

$$\psi_1(\xi, \sigma) = \theta + \vartheta \tan\left(\vartheta \sqrt{-\phi_3}(\varphi - \varphi_0)\right) + \frac{\phi_2}{4}, \tag{3.25}$$

which is a triangular function periodic solution, see Figure 5.

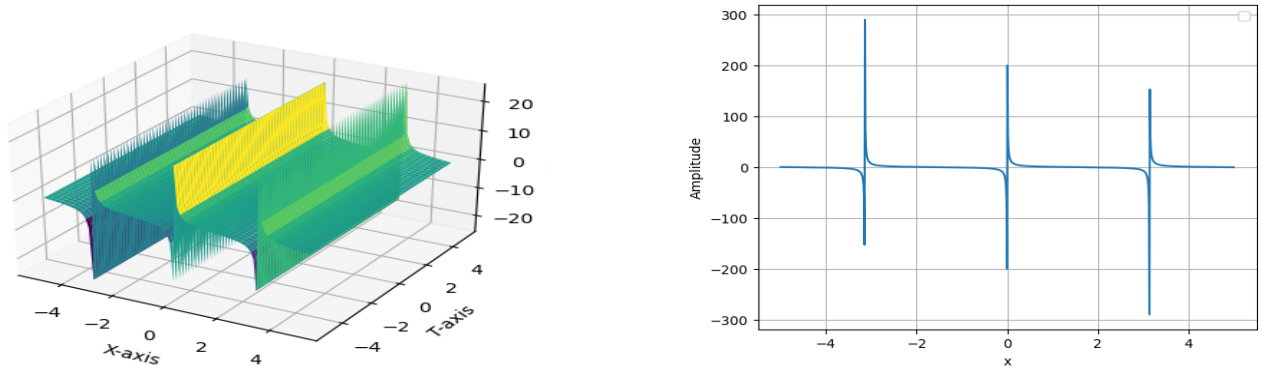

(a) **(b)**

Figure 5. Graph of $\psi_1(x,t)$ in Eq (3.25) is observed, where $\theta = 0.9$, $\vartheta = 0.7$, $\mu = 0.9$, $k_h = 0.9$, $k_c = 1.9$, $\tau = 0.3$, $V = 0.5$, $f = 0.7$, $\alpha = 1$, $\varphi_0 = 0$, $n_0 = 0.1$. (a) 3D plot, (b) 2D graph.

Case 2. $O_2 = 0$, $O_3 = 0$, and $O_4 = 0$. Thus, we have

$$R(L) = L^4. \tag{3.26}$$

When $\phi_3 < 0$, by using Eq (3.8), then, we get

$$L = -\frac{1}{\sqrt{-\phi_3}}(\varphi - \varphi_0)^{-1}. \tag{3.27}$$

Furthermore, we get the solution

$$\psi_1(\xi,\sigma) = -\frac{1}{\sqrt{-\phi_3}}(\varphi - \varphi_0)^{-1} + \frac{\phi_2}{4}, \tag{3.28}$$

which is a rational solution, see Figure 6.

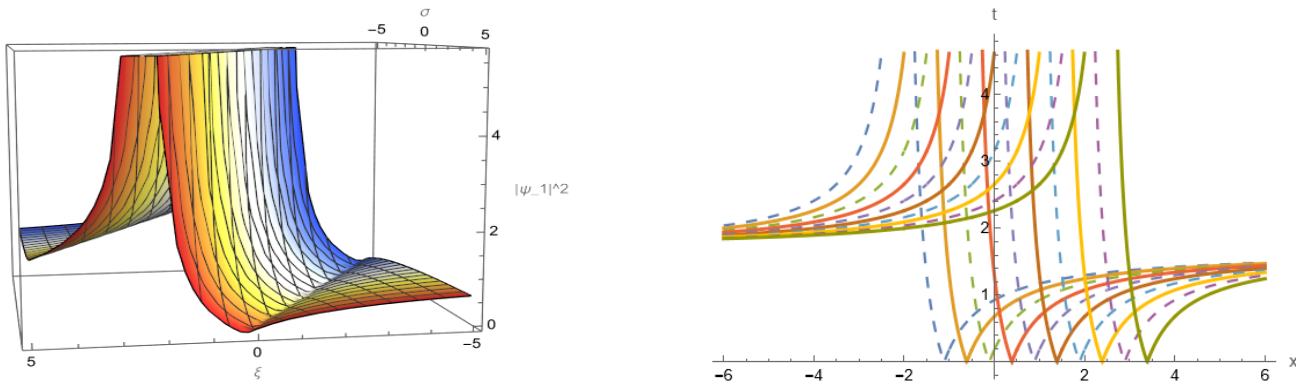

(a) **(b)**

Figure 6. Graph of $\psi_1(x,t)$ in Eq (3.28) is observed, when the variables: $\mu = 0.91$, $k_h = 0.9$, $k_c = 1.9$, $\tau = 0.32$, $V = 0.5$, $f = 0.7$, $\alpha = 1$, $\varphi_0 = 0$, $n_0 = 0.1$. (a) 3D graph, (b) 2D plot.

Case 3. $O_2 > 0$, $O_3 = 0$, $O_4 = 0$, and $H_2 > 0$. Thus, we have

$$R(L) = (L-a)^2(L-b)^2, \tag{3.29}$$

where $a > b$. For $\phi_3 < 0$, from using Eq (3.8), then, we get

$$L = \frac{a-b}{2}(\coth\frac{(a-b)\sqrt{-\phi_3}(\varphi-\varphi_0)}{2} - 1) + b. \tag{3.30}$$

$$L = \frac{b-a}{2}(\tanh\frac{(a-b)\sqrt{-\phi_3}(\varphi-\varphi_0)}{2} - 1) + b. \tag{3.31}$$

In addition, we obtain two solutions

$$\psi_1(\xi,\sigma) = (\frac{a-b}{2}(\coth\frac{(a-b)\sqrt{-\phi_3}(\varphi-\varphi_0)}{2} - 1) + b) + \frac{\phi_2}{4}. \tag{3.32}$$

$$\psi_1(\xi,\sigma) = (\frac{b-a}{2}(\tanh\frac{(a-b)\sqrt{-\phi_3}(\varphi-\varphi_0)}{2} - 1) + b) + \frac{\phi_2}{4}. \tag{3.33}$$

These are solitary wave (SW) solutions, see Figures 7 and 8.

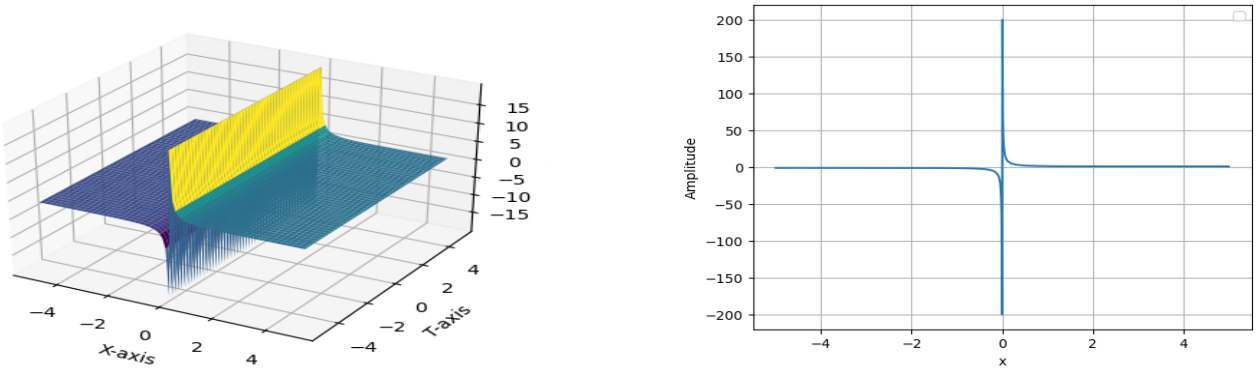

(a) **(b)**

Figure 7. A graph of $\psi_1(x,t)$ is displaced in Eq (3.32), where $a = 2.52$, $b = 1.92$, $\mu = 1.95$, $k_h = 0.3$, $k_c = 1.9$, $\tau = 0.52$, $V = 1.8$, $f = 0.8$, $\alpha = 1$, $\varphi_0 = 0$, $n_0 = 0.1$. (a) 3D display, (b) 2D visual.

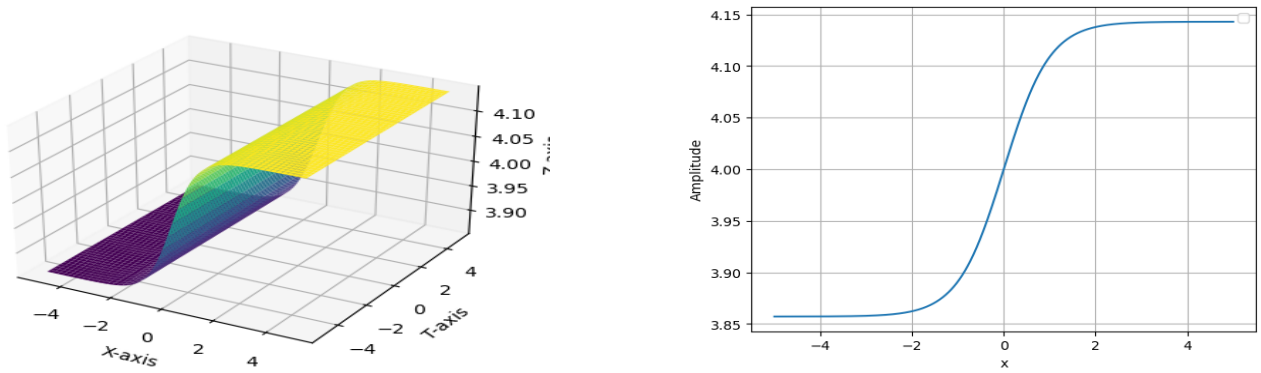

(a) **(b)**

Figure 8. The graphical fluctuation in $\psi_1(x,t)$ as defined in Eq (3.33), where $a = 2.52$, $b = 1.02$, $\mu = 1.95$, $k_h = 0.3$, $k_c = 1.1$, $\tau = 0.52$, $V = 0.8$, $f = 0.8$, $\alpha = 1$, $\varphi_0 = 0$, $n_0 = 0.1$. (a) 3D graph, (b) 2D display.

Case 4. $O_2 > 0$, $O_3 = 0$, $O_4 = 0$, and $H_2 = 0$. Thus, we have

$$R(L) = (L-\zeta)^3(L-\chi). \tag{3.34}$$

For $\phi_3 < 0$, from Eq (3.8), we have

$$L = \frac{4(\zeta-\chi)}{(\chi-\zeta)^2(-\phi_3)(\varphi-\varphi_0)^2-4} + \zeta. \tag{3.35}$$

Since, we obtain the following solution:

$$\psi_1(\xi,\sigma) = \left(\frac{4(\zeta-\chi)}{(\chi-\zeta)^2(-\phi_3)(\varphi-\varphi_0)^2-4} + \zeta\right) + \frac{\phi_2}{4}. \tag{3.36}$$

For $\phi_3 > 0$, then, we can obtain:

$$L = \frac{4(\zeta-\chi)}{-(\chi-\zeta)^2(-\phi_3)(\varphi-\varphi_0)^2-4} + \zeta. \tag{3.37}$$

Hence,

$$\psi_1(\xi,\sigma) = \left(\frac{4(\zeta-\chi)}{-(\chi-\zeta)^2(\phi_3)(\varphi-\varphi_0)^2-4} + \zeta\right) + \frac{\phi_2}{4}. \tag{3.38}$$

Eqs (3.36) and (3.38) are rational solutions, see Figures 9 and 10.

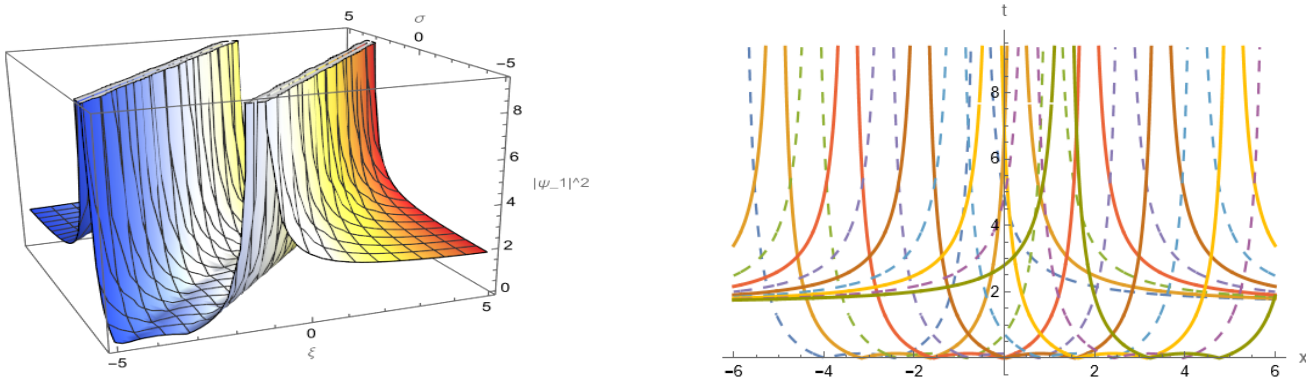

(a) **(b)**

Figure 9. The visual graphics of $\psi_1(x,t)$ using Eq (3.36), where $\zeta = 2.52, \chi = 1.02, \mu = 1.95, k_h = 0.3, k_c = 1.1, \tau = 0.52, V = 0.8, f = 0.8, \alpha = 1, \varphi_0 = 0, n_0 = 0.1$. (a) 3D graph, (b) 2D plot.

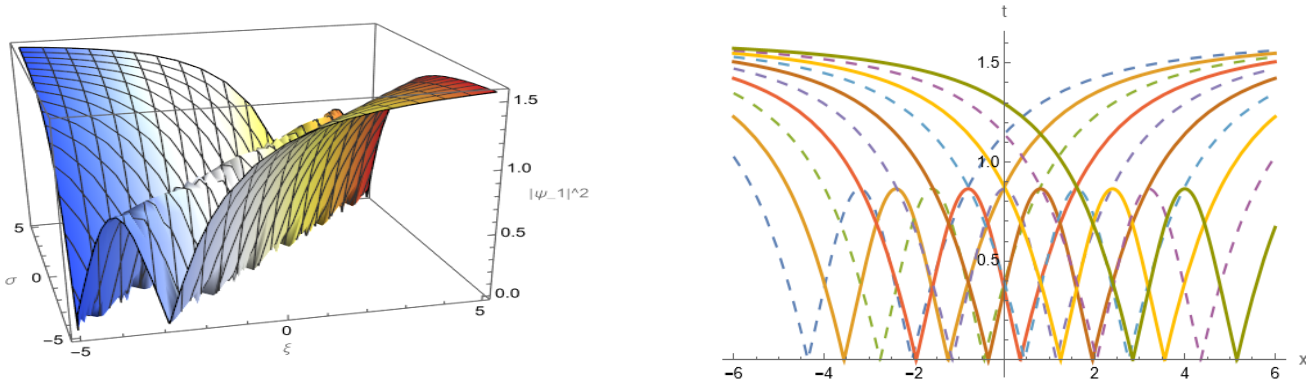

(a) **(b)**

Figure 10. The dynamical behaviour of $\psi_1(x,t)$ using Eq (3.38), where $\zeta = 2.52, \chi = 0.02, \mu = 1.95, k_h = 0.3, k_c = 1.1, \tau = 0.52, V = 0.8, f = 0.8, \alpha = 1, \varphi_0 = 0, n_0 = 0.1$. (a) 3D display, (b) 2D plot.

Case 5. $O_2O_3 < 0$, and $O_4 = 0$. Since,

$$R(L) = (L-\psi)^2((F-A)^2 + B^2). \tag{3.39}$$

Then, we have

$$L = \frac{(\exp^{\pm\sqrt{(\psi-A)^2+B^2}\sqrt{-\phi_3}(\varphi-\varphi_0)} - \varrho) + \sqrt{(\psi-A)^2+B^2}(2-\varrho)}{(\exp^{\pm\sqrt{(\psi-A)^2+B^2}\sqrt{-\phi_3}(\varphi-\varphi_0)} - \varrho)^2 - 1}, \tag{3.40}$$

where $\varrho = \frac{\psi-2A}{\sqrt{(\psi-A)^2+B^2}}$. Since, we have

$$\psi_1(\xi,\sigma) = \frac{(\exp^{\pm\sqrt{(\psi-A)^2+B^2}\sqrt{-\phi_3}(\varphi-\varphi_0)} - \varrho) + \sqrt{(\psi-A)^2+B^2}(2-\varrho)}{(\exp^{\pm\sqrt{(\psi-A)^2+B^2}\sqrt{-\phi_3}(\varphi-\varphi_0)} - \varrho)^2 - 1} + \frac{\phi_2}{4}, \tag{3.41}$$

that is a SW soliton solution, see Figure 11.

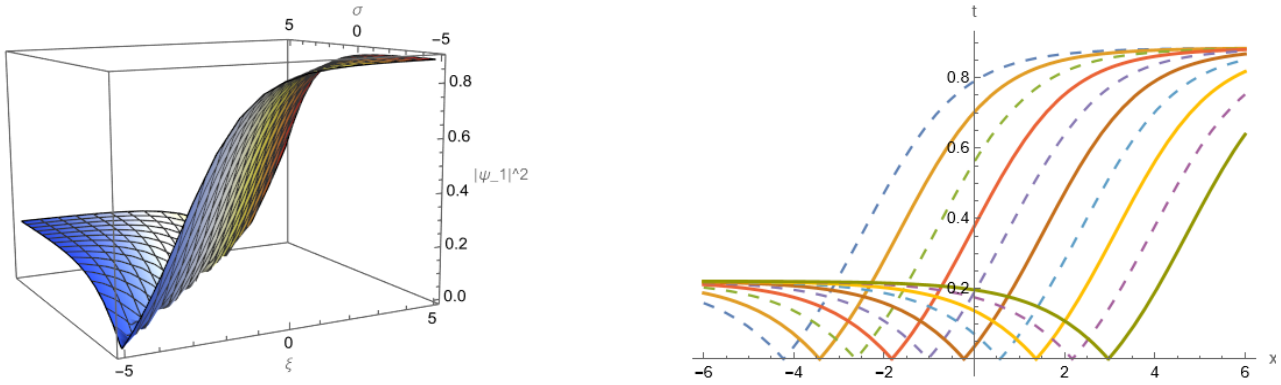

(a) **(b)**

Figure 11. The configuration of $\psi_1(x,t)$ through Eq (3.41) with the given parameters $\psi = 2.4$, $A = 0.93$, $B = 0.4$, $\mu = 1.95$, $k_h = 0.3$, $k_c = 1.1$, $\tau = 0.52$, $V = 0.5$, $f = 0.8$, $\alpha = 1$, $\varphi_0 = 0$, $n_0 = 0.1$. (a) 3D display, (b) 2D visual.

Case 6. $O_2 > 0$, $O_3 > 0$, and $O_4 > 0$. Since, we have

$$R(L) = (L-\lambda_1)(L-\lambda_2)(L-\lambda_3)(L-\lambda_4), \tag{3.42}$$

at which $\lambda_1 > \lambda_2 > \lambda_3 > \lambda_4$. For $\phi_3 < 0$, from Eq (3.8), then, we can get

$$L = \frac{\lambda_2(\lambda_1-\lambda_4)sn^2(\frac{\sqrt{(\lambda_1-\lambda_3)(\lambda_2-\lambda_4)}}{2}\sqrt{-\phi_3}(\varphi-\varphi_0),\varrho) - \lambda_1(\lambda_2-\lambda_4)}{(\lambda_1-\lambda_4)sn^2(\frac{\sqrt{(\lambda_1-\lambda_3)(\lambda_2-\lambda_4)}}{2}\sqrt{-\phi_3}(\varphi-\varphi_0),\varrho) - (\lambda_2-\lambda_4)}, \tag{3.43}$$

$$L = \frac{\lambda_4(\lambda_2-\lambda_3)sn^2(\frac{\sqrt{(\lambda_1-\lambda_3)(\lambda_2-\lambda_4)}}{2}\sqrt{-\phi_3}(\varphi-\varphi_0),\varrho) - \lambda_3(\lambda_2-\lambda_4)}{(\lambda_2-\lambda_3)sn^2(\frac{\sqrt{(\lambda_1-\lambda_3)(\lambda_2-\lambda_4)}}{2}\sqrt{-\phi_3}(\varphi-\varphi_0),\varrho) - (\lambda_2-\lambda_4)}, \tag{3.44}$$

where $\varrho = \frac{(\lambda_1-\lambda_4)(\lambda_2-\lambda_3)}{(\lambda_1-\lambda_3)(\lambda_2-\lambda_4)}$. Since, we can find the two solutions

$$\psi_1(\xi,\sigma) = \frac{\lambda_2(\lambda_1-\lambda_4)sn^2(\frac{\sqrt{(\lambda_1-\lambda_3)(\lambda_2-\lambda_4)}}{2}\sqrt{-\phi_3}(\varphi-\varphi_0),\varrho) - \lambda_1(\lambda_2-\lambda_4)}{(\lambda_1-\lambda_4)sn^2(\frac{\sqrt{(\lambda_1-\lambda_3)(\lambda_2-\lambda_4)}}{2}\sqrt{-\phi_3}(\varphi-\varphi_0),\varrho) - (\lambda_2-\lambda_4)} + \frac{\phi_2}{4}. \tag{3.45}$$

$$\psi_1(\xi,\sigma) = \frac{\lambda_4(\lambda_2-\lambda_3)sn^2(\frac{\sqrt{(\lambda_1-\lambda_3)(\lambda_2-\lambda_4)}}{2}\sqrt{-\phi_3}(\varphi-\varphi_0),\varrho) - \lambda_3(\lambda_2-\lambda_4)}{(\lambda_2-\lambda_3)sn^2(\frac{\sqrt{(\lambda_1-\lambda_3)(\lambda_2-\lambda_4)}}{2}\sqrt{-\phi_3}(\varphi-\varphi_0),\varrho) - (\lambda_2-\lambda_4)} + \frac{\phi_2}{4}. \tag{3.46}$$

For $\phi_3 > 0$, from Eq (3.8), then, we can get

$$L = \frac{\lambda_3(\lambda_1-\lambda_2)sn^2(\frac{\sqrt{(\lambda_1-\lambda_3)(\lambda_2-\lambda_4)}}{2}\sqrt{-\phi_3}(\varphi-\varphi_0),\varrho) - \lambda_2(\lambda_1-\lambda_3)}{(\lambda_1-\lambda_2)sn^2(\frac{\sqrt{(\lambda_1-\lambda_3)(\lambda_2-\lambda_4)}}{2}\sqrt{-\phi_3}(\varphi-\varphi_0),\varrho) - (\lambda_1-\lambda_3)}, \tag{3.47}$$

$$L = \frac{\lambda_1(\lambda_3-\lambda_4)sn^2(\frac{\sqrt{(\lambda_1-\lambda_3)(\lambda_2-\lambda_4)}}{2}\sqrt{-\phi_3}(\varphi-\varphi_0),\varrho)-\lambda_4(\lambda_3-\lambda_1)}{(\lambda_3-\lambda_4)sn^2(\frac{\sqrt{(\lambda_1-\lambda_3)(\lambda_2-\lambda_4)}}{2}\sqrt{-\phi_3}(\varphi-\varphi_0),\varrho)-(\lambda_3-\lambda_1)}, \tag{3.48}$$

where $\varrho = \frac{(\lambda_1-\lambda_2)(\lambda_3-\lambda_4)}{(\lambda_1-\lambda_3)(\lambda_2-\lambda_4)}$. Since, we get the two solutions

$$\psi_1(\xi,\sigma) = \frac{\lambda_3(\lambda_1-\lambda_2)sn^2(\frac{\sqrt{(\lambda_1-\lambda_3)(\lambda_2-\lambda_4)}}{2}\sqrt{-\phi_3}(\varphi-\varphi_0),\varrho)-\lambda_2(\lambda_1-\lambda_3)}{(\lambda_1-\lambda_2)sn^2(\frac{\sqrt{(\lambda_1-\lambda_3)(\lambda_2-\lambda_4)}}{2}\sqrt{-\phi_3}(\varphi-\varphi_0),\varrho)-(\lambda_1-\lambda_3)}+\frac{\phi_2}{4}. \tag{3.49}$$

$$\psi_1(\xi,\sigma) = \frac{\lambda_1(\lambda_3-\lambda_4)sn^2(\frac{\sqrt{(\lambda_1-\lambda_3)(\lambda_2-\lambda_4)}}{2}\sqrt{-\phi_3}(\varphi-\varphi_0),\varrho)-\lambda_4(\lambda_3-\lambda_1)}{(\lambda_3-\lambda_4)sn^2(\frac{\sqrt{(\lambda_1-\lambda_3)(\lambda_2-\lambda_4)}}{2}\sqrt{-\phi_3}(\varphi-\varphi_0),\varrho)-(\lambda_3-\lambda_1)}+\frac{\phi_2}{4}. \tag{3.50}$$

Equations (3.45), (3.46), (3.49), and (3.50) are a JEF double periodic solutions, see Figures 12–15.

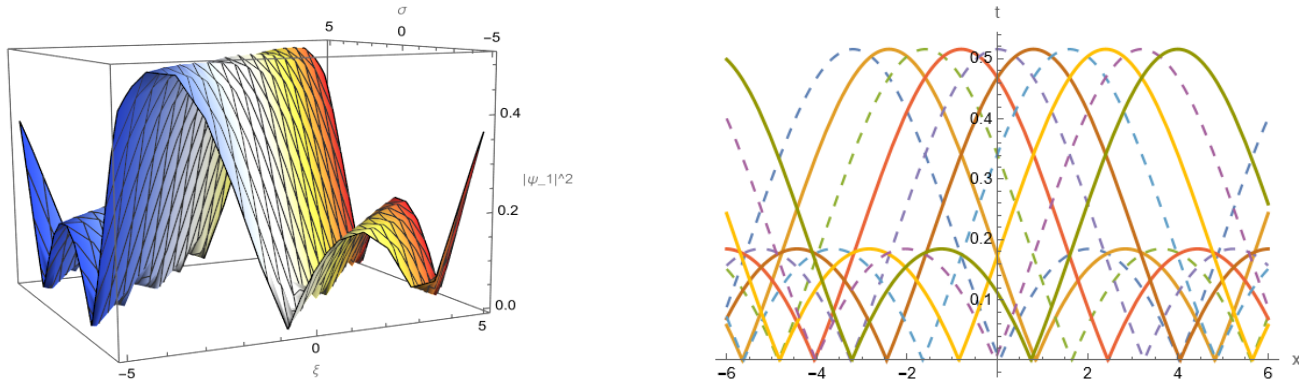

(a) **(b)**

Figure 12. The shape profile of $\psi_1(x,t)$ to Eq (3.45) with parameters $\lambda_1 = 1.4$, $\lambda_2 = 0.7$, $\lambda_3 = 2.8$, $\lambda_4 = 0.19$, $\mu = 1.95$, $k_h = 0.3$, $k_c = 1.1$, $\tau = 0.52$, $V = 0.5$, $f = 0.8$, $\alpha = 1$, $\varphi_0 = 0$, $n_0 = 0.1$. (a) 3D graph, (b) 2D visual.

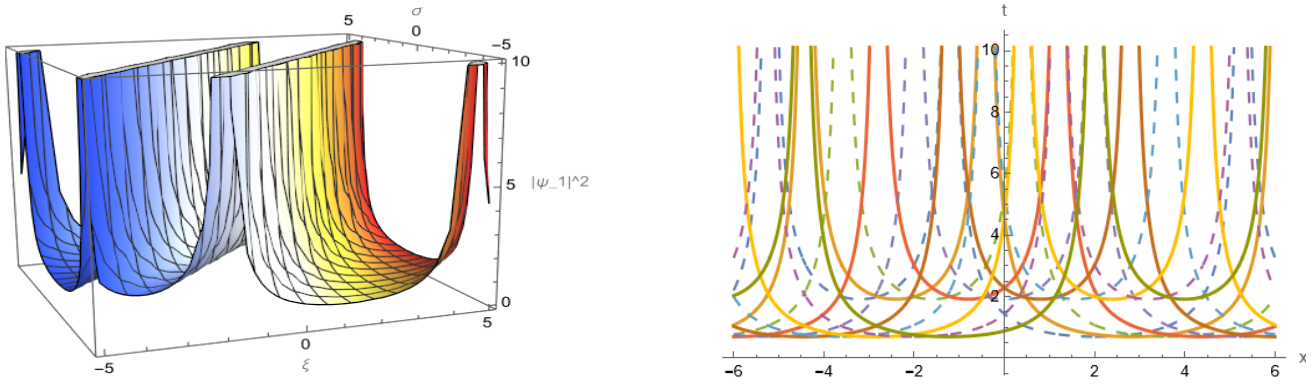

(a) **(b)**

Figure 13. The dynamical analysis of $\psi_1(x,t)$ given by Eq (3.46) with values $\lambda_1 = 1.4$, $\lambda_2 = 0.7$, $\lambda_3 = 2.8$, $\lambda_4 = 0.19$, $\mu = 1.95$, $k_h = 0.3$, $k_c = 1.1$, $\tau = 0.52$, $V = 0.5$, $f = 0.8$, $\alpha = 1$, $\varphi_0 = 0$, $n_0 = 0.1$. (a) 3D display, (b) 2D plot.

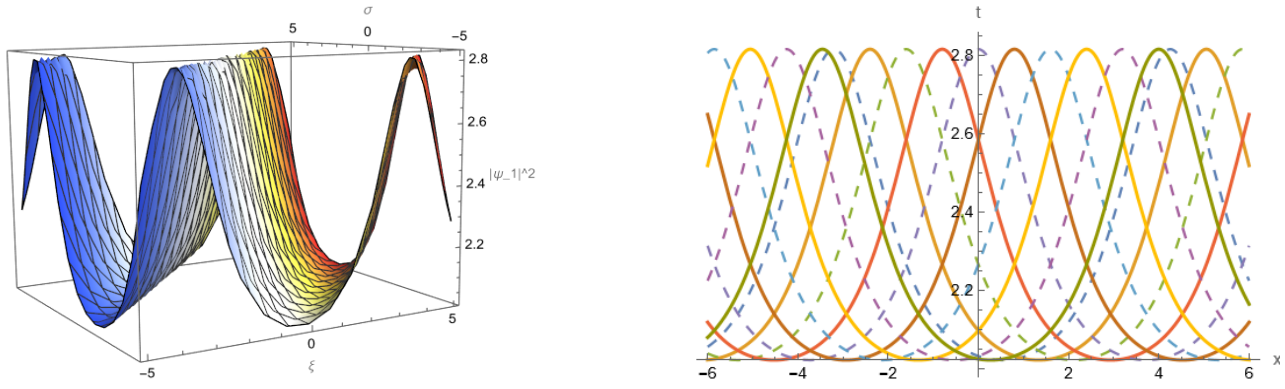

(a) **(b)**

Figure 14. The dynamical analysis of $\psi_1(x,t)$ given by Eq (3.46) with values $\lambda_1 = 1.4$, $\lambda_2 = 0.7$, $\lambda_3 = 2.8$, $\lambda_4 = 0.19$, $\mu = 1.95$, $k_h = 0.3$, $k_c = 1.1$, $\tau = 0.52$, $V = 0.5$, $f = 0.8$, $\alpha = 1$, $\varphi_0 = 0$, $n_0 = 0.1$. (a) 3D display, (b) 2D plot.

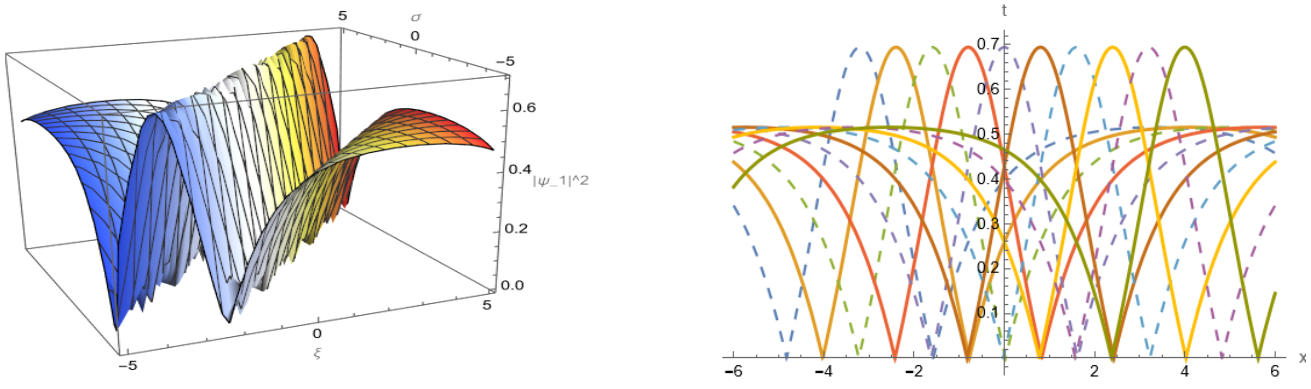

(a) **(b)**

Figure 15. Using Eq (3.50) generate an illustration of $\psi_1(x,t)$ with the following parameters: $\lambda_1 = 1.4$, $\lambda_2 = 2.7$, $\lambda_3 = 2.8$, $\lambda_4 = 0.19$, $\mu = 1.95$, $k_h = 0.3$, $k_c = 1.1$, $\tau = 0.52$, $V = 0.5$, $f = 0.8$, $\alpha = 1$, $\varphi_0 = 0$, $n_0 = 0.1$. (a) 3D graph, (b) 2D visual.

Case 7. $O_2O_3 \geq 0$, and $O_4 < 0$. So, we have

$$R(L) = (L-\psi)(L-\nu)((L-\Theta)^2 + q^2), \tag{3.51}$$

wherever $\Psi > \Gamma$, $l > 0$, $\theta > 0$. Then, we denote

$$\begin{aligned} v &= \frac{1}{2}(\Psi+\nu)n - \frac{1}{2}(\Psi-\nu)f, \\ o &= \frac{1}{2}(\Psi+\nu)f - \frac{1}{2}(\Psi-\nu)n, \\ k &= \Psi - \Theta - \frac{q}{\varrho_1}, \\ h &= \Psi - \Theta - q\varrho_1, \\ S &= \frac{q^2 + (\Psi-\Theta)(\Psi-\nu)}{q(\Psi-\nu)}, \end{aligned} \tag{3.52}$$

$$\varrho_1 = S \pm \sqrt{S^2+1},$$
$$\varrho^2 = \frac{1}{1+\varrho_1}.$$

Then, we have

$$L = \frac{vcn(\frac{\sqrt{\mp 2q\varrho_1(\Psi-\nu)}}{2\varrho\varrho_1}\sqrt{-\phi_3}(\varphi-\varphi_0),\varrho)+o}{kcn(\frac{\sqrt{\mp 2q\varrho_1(\Psi-\nu)}}{2\varrho\varrho_1}\sqrt{-\phi_3}(\varphi-\varphi_0),\varrho)+h}. \tag{3.53}$$

Furthermore, we have the following solution

$$\psi_1(\xi,\sigma) = \frac{vcn(\frac{\sqrt{\mp 2q\varrho_1(\Psi-\nu)}}{2\varrho\varrho_1}\sqrt{-\phi_3}(\varphi-\varphi_0),\varrho)+o}{kcn(\frac{\sqrt{\mp 2q\varrho_1(\Psi-\nu)}}{2\varrho\varrho_1}\sqrt{-\phi_3}(\varphi-\varphi_0),\varrho)+h} + \frac{\phi_2}{4}, \tag{3.54}$$

that is a JEF double periodic solution, see Figure 16.

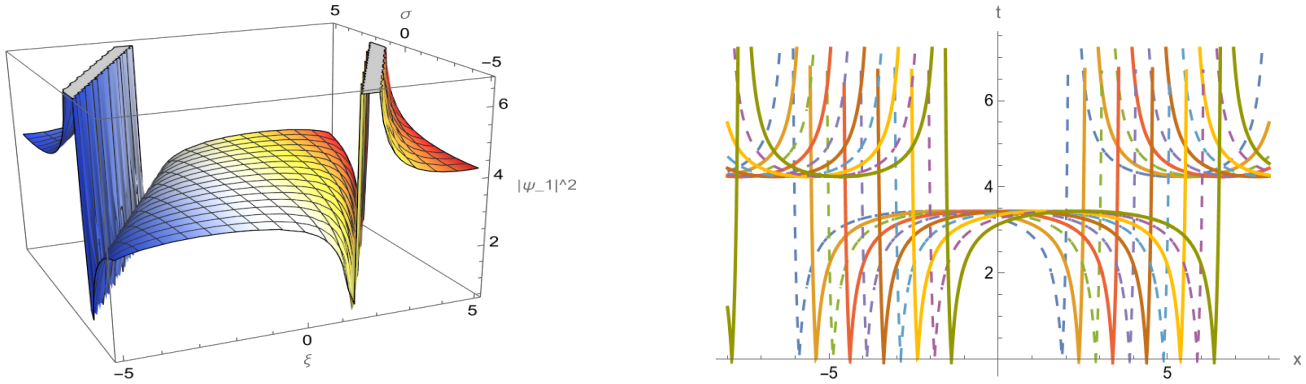

(a) **(b)**

Figure 16. The graphical structure of $\psi_1(x,t)$ by Eq (3.54) with the parameters $\Psi = 2.5$, $\nu = 1.7$, $\Theta = 2.87$, $q = 1.2$, $\mu = 0.9$, $k_h = 0.9$, $k_c = 1.9$, $\tau = 0.3$, $V = 0.5$, $f = 0.7$, $\alpha = 1$, $\varphi_0 = 0$, $n_0 = 0.1$. (a) 3D graph, (b) 2D plot.

Case 8. $O_2O_3 \leq 0$, and $O_4 > 0$. So, we have

$$R(L) = ((L-r_1)^2 + w_1^2)((L-r_2)^2 + w_2^2), \tag{3.55}$$

where $w_1 \geq w_2 > 0$. We denote

$$\begin{aligned} c &= r_1 h + w_1 k \\ e &= r_1 k - w_1 h, \\ h &= -w_1 - \frac{w_2}{\varrho_1}, \\ k &= r_1 - r_2, \\ S &= \frac{(r_1-r_2)^2 + w_1^2 + w_2^2}{2w_1 w_2}, \end{aligned} \tag{3.56}$$

$$\varrho_1 = S + \sqrt{S^2 - 1},$$
$$\varrho^2 = \frac{\varrho_1^2 - 1}{\varrho_1^2}.$$

Then, we have

$$L = \frac{csn(\eta\sqrt{-\phi_3}(\varphi - \varphi_0), \varrho) + ecn(\eta\sqrt{-\phi_3}(\varphi - \varphi_0), \varrho)}{hsn(\eta\sqrt{-\phi_3}(\varphi - \varphi_0), \varrho) + kcn(\eta\sqrt{-\phi_3}(\varphi - \varphi_0), \varrho)}, \tag{3.57}$$

where $\eta = \frac{w_2\sqrt{(h^2+k^2)(\delta_1^2h^2+k^2)}}{h^2+k^2}$. Moreover, we have

$$\psi_1(x,t) = \frac{csn(\eta\sqrt{-\phi_3}(\varphi - \varphi_0), \varrho) + ecn(\eta\sqrt{-\phi_3}(\varphi - \varphi_0), \varrho)}{hsn(\eta\sqrt{-\phi_3}(\varphi - \varphi_0), \varrho) + kcn(\eta\sqrt{-\phi_3}(\varphi - \varphi_0), \varrho)} + \frac{\phi_2}{4}, \tag{3.58}$$

that is a JEF double periodic solution, see Figure 17.

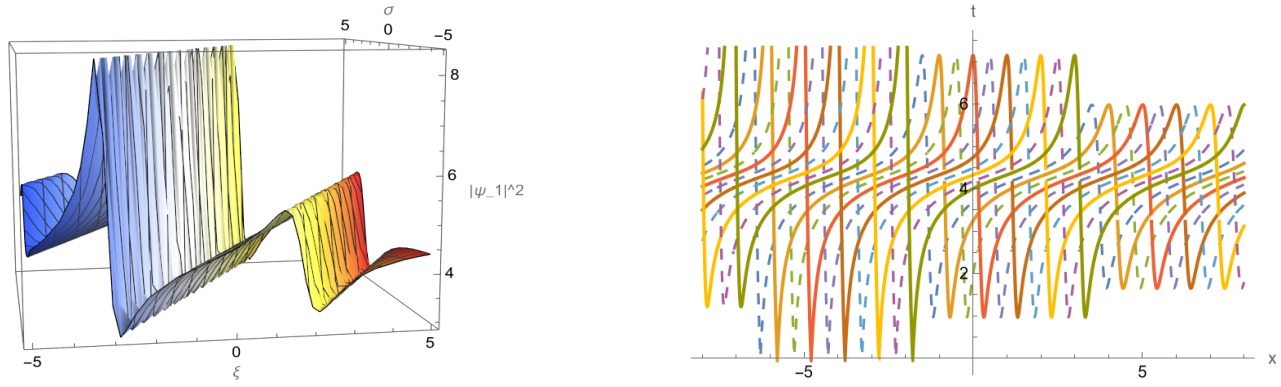

(a) **(b)**

Figure 17. A graphical illustration of $\psi_1(x,t)$ to Eq (3.58) with values $r_1 = 2.5$, $r_2 = 1.7$, $w_1 = 0.87$, $w_2 = 1.2$, $\mu = 0.9$, $k_h = 0.9$, $k_c = 1.9$, $\tau = 0.3$, $V = 0.5$, $f = 0.7$, $\alpha = 1$, $\varphi_0 = 0$, $n_0 = 0.1$. (a) 3D display, (b) 2D visual.

Case 9. $D_3 > 0$, $D_4 = 0$, and $D_2 > 0$. Thus, we have

$$R(L) = (L - \tau_1)^2(L - \tau_2)(L - \tau_3), \tag{3.59}$$

where τ_1, τ_2, and τ_3 are real numbers, $\tau_1 = \frac{-\tau_2+\tau_3}{2}$ and $w = (\tau_1 - \tau_2)(\tau_1 - \tau_3)$.

If $L > \tau_2$ and $\tau_2 > \tau_1 > \tau_3$, then, we have,

$$L = \frac{2w}{(\tau_2 - \tau_3)\sinh(\sqrt{-w}\sqrt{-\phi_3}(\varphi - \varphi_0)) + 2\tau_2}. \tag{3.60}$$

If $\tau_1 > \tau_2$ and $\tau_1 < \tau_3$, thus, we have

$$L = \frac{2w}{(\tau_2 - \tau_3)\cosh(\sqrt{w}\sqrt{-\phi_3}(\varphi - \varphi_0)) + 2\tau_2}. \tag{3.61}$$

Furthermore, we get the two solutions

$$\psi_1(\xi,\sigma) = \left(\frac{2w}{(\tau_2-\tau_3)\cosh(\sqrt{w}\sqrt{-\phi_3}(\varphi-\varphi_0))+2\tau_2}\right)+\frac{\phi_2}{4}. \tag{3.62}$$

$$\psi_1(\xi,\sigma) = \left(\frac{2w}{(\tau_2-\tau_3)\cosh(\sqrt{w}\sqrt{-\phi_3}(\varphi-\varphi_0))+2\tau_2}\right)+\frac{\phi_2}{4}. \tag{3.63}$$

Equations (3.62) and (3.63) are a SW solutions, see Figures 18 and 19.

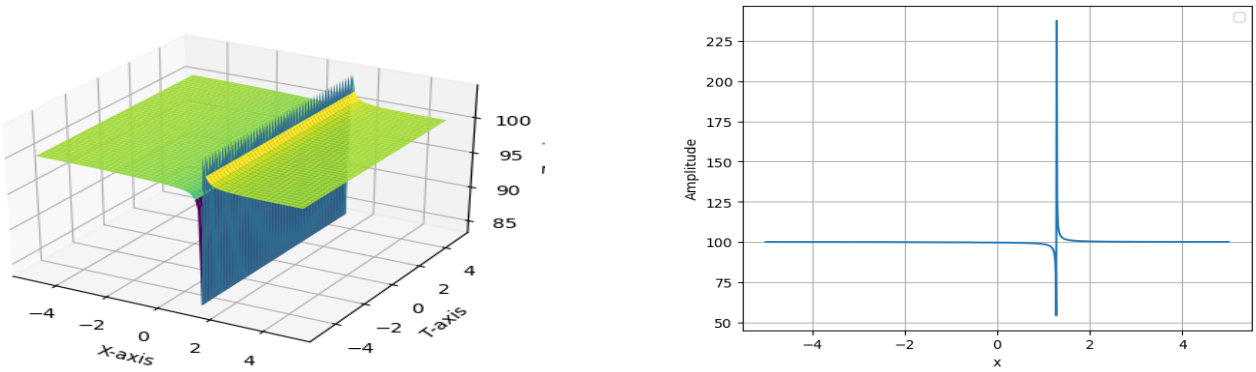

(a) **(b)**

Figure 18. A graphs of $\psi_1(x,t)$ to Eq (3.62) with values: $\tau_2 = 1.3$, $\tau_3 = 2.3$, $\mu = 0.9$, $k_h = 0.9$, $k_c = 1.9$, $\tau = 0.3$, $V = 0.5$, $f = 0.7$, $\alpha = 1$, $\varphi_0 = 0$, $n_0 = 0.1$. (a) 3D plot, (b) 2D graph.

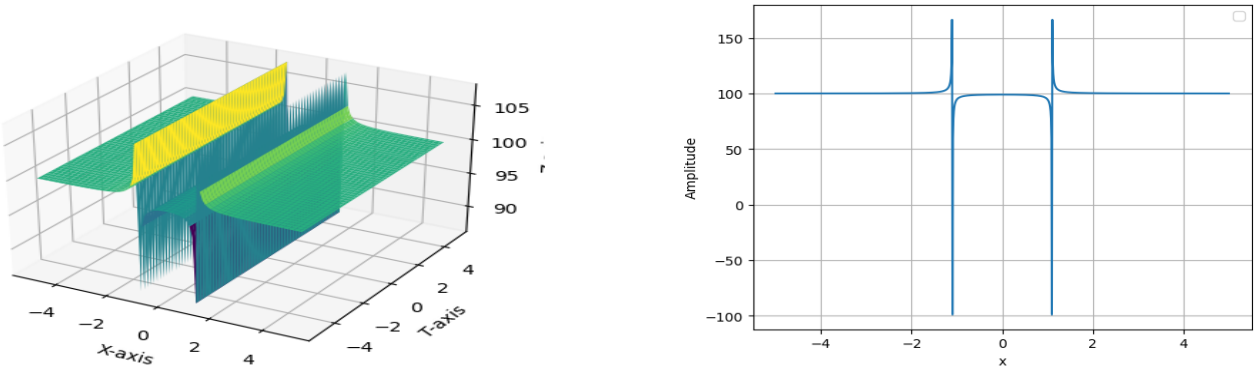

(a) **(b)**

Figure 19. A graphical illustration of $\psi_1(x,t)$ to Eq (3.63) with values: $\tau_2 = 1.3$, $\tau_3 = 2.3$, $\mu = 0.9$, $k_h = 0.9$, $k_c = 1.9$, $\tau = 0.3$, $V = 0.5$, $f = 0.7$, $\alpha = 1$, $\varphi_0 = 0$, $n_0 = 0.1$. (a) 3D graph, (b) 2D visual.

4. The SW solutions

It is intriguing to explore many exact and explicit local pulse solutions that are disseminated over a fiber optic system. We solve SW in this section with trigonometric and HF derived from JEF. The

JEF is converted into trigonometric and HF that converge to $\varrho \to 0$ and $\varrho \to 1$, respectively, in the long-wave approximation.

4.1. Two-fold HF

By containing the limit $\varrho \to 1$ in Eqs (3.45), (3.46), (3.49), and (3.50), then, the function degenerate into

$$sn^2\left(\frac{\sqrt{(\lambda_1-\lambda_3)(\lambda_2-\lambda_4)}}{2}\sqrt{-\phi_3}(\varphi-\varphi_0),\varrho\right) \to \tanh^2\left(\frac{\sqrt{(\lambda_1-\lambda_3)(\lambda_2-\lambda_4)}}{2}\sqrt{-\phi_3}(\varphi-\varphi_0)\right),$$

which present the SWs solution [39], see Figures 20 and 21.

$$\psi_1(\xi,\sigma) = \frac{\lambda_2(\lambda_1-\lambda_4)\tanh^2\left(\frac{\sqrt{(\lambda_1-\lambda_3)(\lambda_2-\lambda_4)}}{2}\sqrt{-\phi_3}(\varphi-\varphi_0)\right)-\lambda_1(\lambda_2-\lambda_4)}{(\lambda_1-\lambda_4)\tanh^2\left(\frac{\sqrt{(\lambda_1-\lambda_3)(\lambda_2-\lambda_4)}}{2}\sqrt{-\phi_3}(\varphi-\varphi_0)\right)-(\lambda_2-\lambda_4)}+\frac{\phi_2}{4}. \tag{4.1}$$

$$\psi_1(\xi,\sigma) = \frac{\lambda_4(\lambda_2-\lambda_3)\tanh^2\left(\frac{\sqrt{(\lambda_1-\lambda_3)(\lambda_2-\lambda_4)}}{2}\sqrt{-\phi_3}(\varphi-\varphi_0)\right)-\lambda_3(\lambda_2-\lambda_4)}{(\lambda_2-\lambda_3)\tanh^2\left(\frac{\sqrt{(\lambda_1-\lambda_3)(\lambda_2-\lambda_4)}}{2}\sqrt{-\phi_3}(\varphi-\varphi_0)\right)-(\lambda_2-\lambda_4)}+\frac{\phi_2}{4}. \tag{4.2}$$

$$\psi_1(\xi,\sigma) = \frac{\lambda_3(\lambda_1-\lambda_2)\tanh^2\left(\frac{\sqrt{(\lambda_1-\lambda_3)(\lambda_2-\lambda_4)}}{2}\sqrt{-\phi_3}(\varphi-\varphi_0)\right)-\lambda_2(\lambda_1-\lambda_3)}{(\lambda_1-\lambda_2)\tanh^2\left(\frac{\sqrt{(\lambda_1-\lambda_3)(\lambda_2-\lambda_4)}}{2}\sqrt{-\phi_3}(\varphi-\varphi_0)\right)-(\lambda_1-\lambda_3)}+\frac{\phi_2}{4}. \tag{4.3}$$

$$\psi_1(\xi,\sigma) = \frac{\lambda_1(\lambda_3-\lambda_4)\tanh^2\left(\frac{\sqrt{(\lambda_1-\lambda_3)(\lambda_2-\lambda_4)}}{2}\sqrt{-\phi_3}(\varphi-\varphi_0)\right)-\lambda_4(\lambda_3-\lambda_1)}{(\lambda_3-\lambda_4)\tanh^2\left(\frac{\sqrt{(\lambda_1-\lambda_3)(\lambda_2-\lambda_4)}}{2}\sqrt{-\phi_3}(\varphi-\varphi_0)\right)-(\lambda_3-\lambda_1)}+\frac{\phi_2}{4}. \tag{4.4}$$

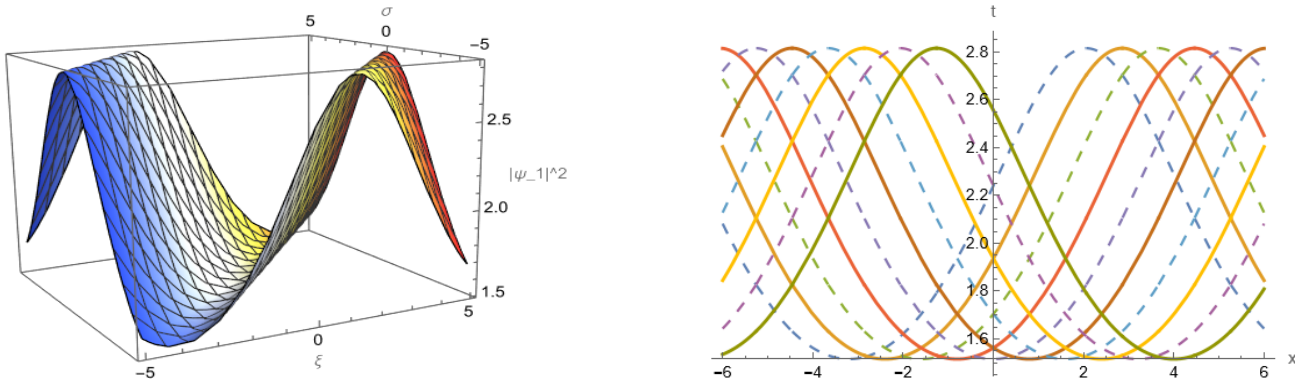

(a) **(b)**

Figure 20. Equation (4.3) provides the figure of $\psi_1(x,t)$, when $\lambda_1 = 0.4$, $\lambda_2 = 3.7$, $\lambda_3 = 2.8$, $\lambda_4 = 1.19$, $\mu = 1.95$, $k_h = 0.3$, $k_c = 1.1$, $\tau = 0.52$, $V = 0.5$, $f = 0.8$, $\alpha = 1$, $\varphi_0 = 0$, $n_0 = 0.1$. (a) 3D plot, (b) 2D visual.

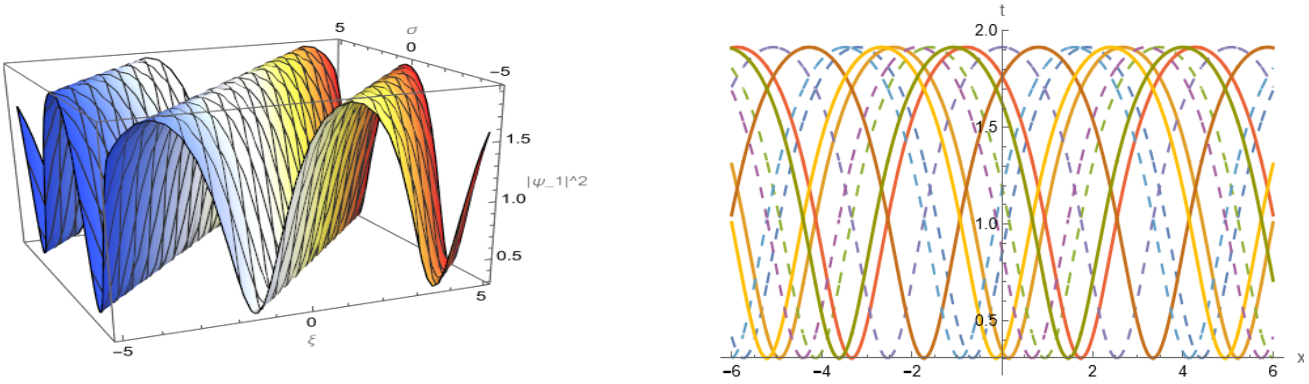

(a) **(b)**

Figure 21. Equation (4.4) provides a dynamical behaviour of $\psi_1(x,t)$, when: $\lambda_1 = 2.4$, $\lambda_2 = 1.7$, $\lambda_3 = 2.8$, $\lambda_4 = 1.19$, $\mu = 1.95$, $k_h = 0.3$, $k_c = 1.1$, $\tau = 0.52$, $V = 0.8$, $f = 0.8$, $\alpha = 1$, $\varphi_0 = 0$, $n_0 = 0.1$. (a) 3D display, (b) 2D graph.

4.2. Two-fold periodic SW (PSW)

By containing the limit $\varrho \to 0$ in Eqs (3.45), (3.46), (3.49), and (3.50), then the function converts into

$$sn^2(\tfrac{\sqrt{(\lambda_1-\lambda_3)(\lambda_2-\lambda_4)}}{2}\sqrt{-\phi_3}(\varphi-\varphi_0),\varrho) \to \sin^2(\tfrac{\sqrt{(\lambda_1-\lambda_3)(\lambda_2-\lambda_4)}}{2}\sqrt{-\phi_3}(\varphi-\varphi_0)),$$

which displays the SW solutions [39], see Figures 22–25.

$$\psi_1(\xi,\sigma) = \frac{\lambda_2(\lambda_1-\lambda_4)\sin^2(\frac{\sqrt{(\lambda_1-\lambda_3)(\lambda_2-\lambda_4)}}{2}\sqrt{-\phi_3}(\varphi-\varphi_0)) - \lambda_1(\lambda_2-\lambda_4)}{(\lambda_1-\lambda_4)\sin^2(\frac{\sqrt{(\lambda_1-\lambda_3)(\lambda_2-\lambda_4)}}{2}\sqrt{-\phi_3}(\varphi-\varphi_0)) - (\lambda_2-\lambda_4)} + \frac{\phi_2}{4}. \tag{4.5}$$

$$\psi_1(\xi,\sigma) = \frac{\lambda_4(\lambda_2-\lambda_3)\sin^2(\frac{\sqrt{(\lambda_1-\lambda_3)(\lambda_2-\lambda_4)}}{2}\sqrt{-\phi_3}(\varphi-\varphi_0)) - \lambda_3(\lambda_2-\lambda_4)}{(\lambda_2-\lambda_3)\sin^2(\frac{\sqrt{(\lambda_1-\lambda_3)(\lambda_2-\lambda_4)}}{2}\sqrt{-\phi_3}(\varphi-\varphi_0)) - (\lambda_2-\lambda_4)} + \frac{\phi_2}{4}. \tag{4.6}$$

$$\psi_1(\xi,\sigma) = \frac{\lambda_3(\lambda_1-\lambda_2)\sin^2(\frac{\sqrt{(\lambda_1-\lambda_3)(\lambda_2-\lambda_4)}}{2}\sqrt{-\phi_3}(\varphi-\varphi_0)) - \lambda_2(\lambda_1-\lambda_3)}{(\lambda_1-\lambda_2)\sin^2(\frac{\sqrt{(\lambda_1-\lambda_3)(\lambda_2-\lambda_4)}}{2}\sqrt{-\phi_3}(\varphi-\varphi_0)) - (\lambda_1-\lambda_3)} + \frac{\phi_2}{4}. \tag{4.7}$$

$$\psi_1(\xi,\sigma) = \frac{\lambda_1(\lambda_3-\lambda_4)\sin^2(\frac{\sqrt{(\lambda_1-\lambda_3)(\lambda_2-\lambda_4)}}{2}\sqrt{-\phi_3}(\varphi-\varphi_0)) - \lambda_4(\lambda_3-\lambda_1)}{(\lambda_3-\lambda_4)\sin^2(\frac{\sqrt{(\lambda_1-\lambda_3)(\lambda_2-\lambda_4)}}{2}\sqrt{-\phi_3}(\varphi-\varphi_0)) - (\lambda_3-\lambda_1)} + \frac{\phi_2}{4}. \tag{4.8}$$

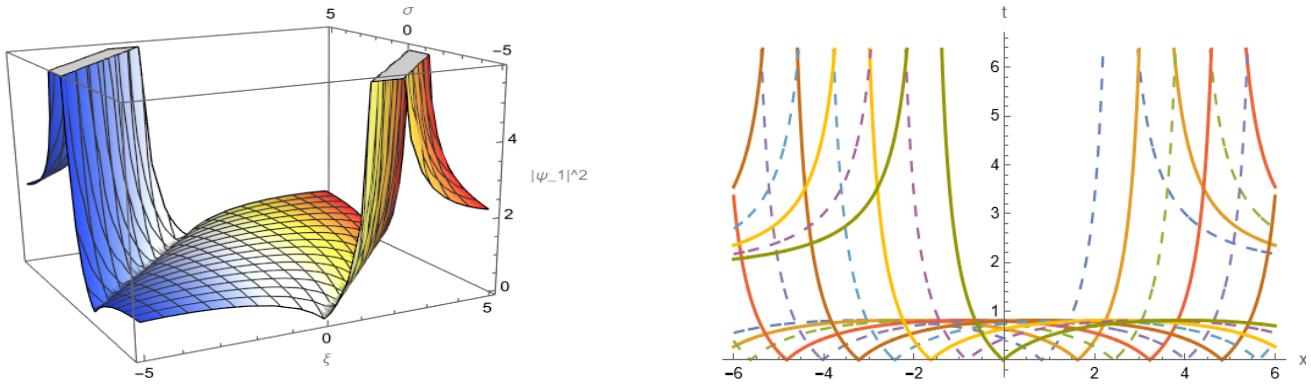

(a) **(b)**

Figure 22. Equation (4.5) provides a representation of $\psi_1(x,t)$, where $\lambda_1 = 2.4$, $\lambda_2 = 2.7$, $\lambda_3 = 0.8$, $\lambda_4 = 1.5$, $\mu = 1.95$, $k_h = 0.3$, $k_c = 1.1$, $\tau = 0.52$, $V = 0.8$, $f = 0.8$, $\alpha = 1$, $\varphi_0 = 0$, $n_0 = 0.1$. (a) 3D plot, (b) 2D visualisation.

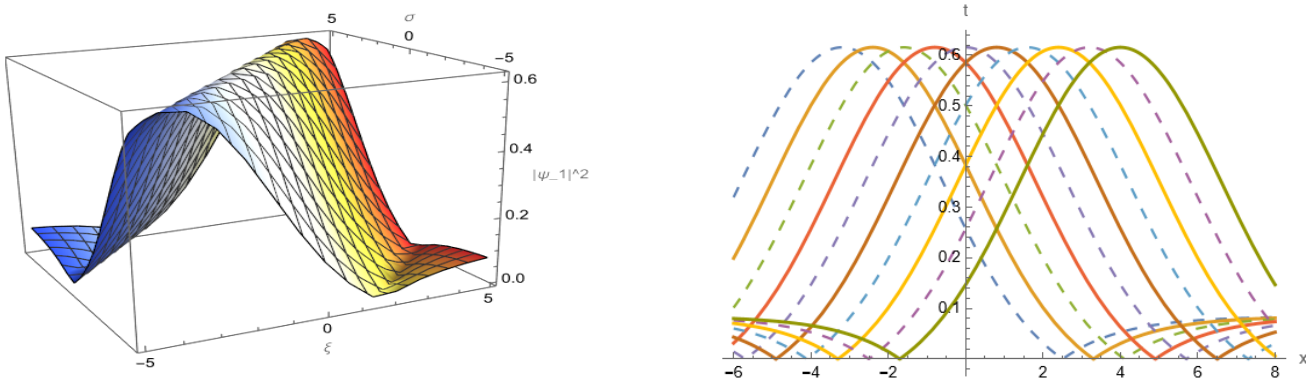

(a) **(b)**

Figure 23. $\psi_1(x,t)$ can be observed graphically in Eq (4.6), if $\lambda_1 = 2.4$, $\lambda_2 = 3.7$, $\lambda_3 = 2.8$, $\lambda_4 = 0.19$, $\mu = 1.95$, $k_h = 0.3$, $k_c = 1.1$, $\tau = 0.52$, $V = 0.8$, $f = 0.8$, $\alpha = 1$, $\varphi_0 = 0$, $n_0 = 0.1$. (a) 3D visualisation, (b) 2D plot.

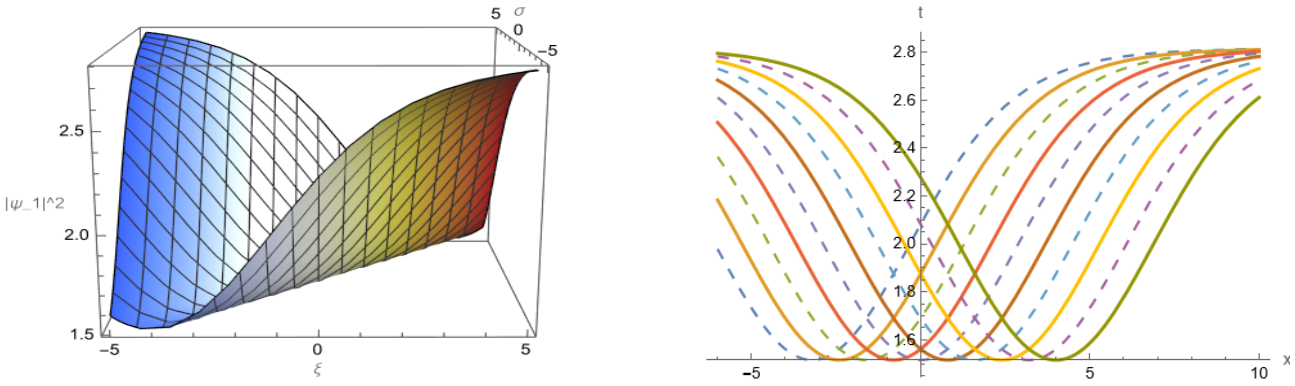

(a) **(b)**

Figure 24. The optical behaviour of $\psi_1(x,t)$ is expressed by Eq (4.7) occurs, when $\lambda_1 = 2.4$, $\lambda_2 = 3.7$, $\lambda_3 = 2.8$, $\lambda_4 = 0.19$, $\mu = 1.95$, $k_h = 0.3$, $k_c = 1.1$, $\tau = 0.52$, $V = 0.8$, $f = 0.8$, $\alpha = 1$, $\varphi_0 = 0$, $n_0 = 0.1$. (a) 3D display, (b) 2D plot.

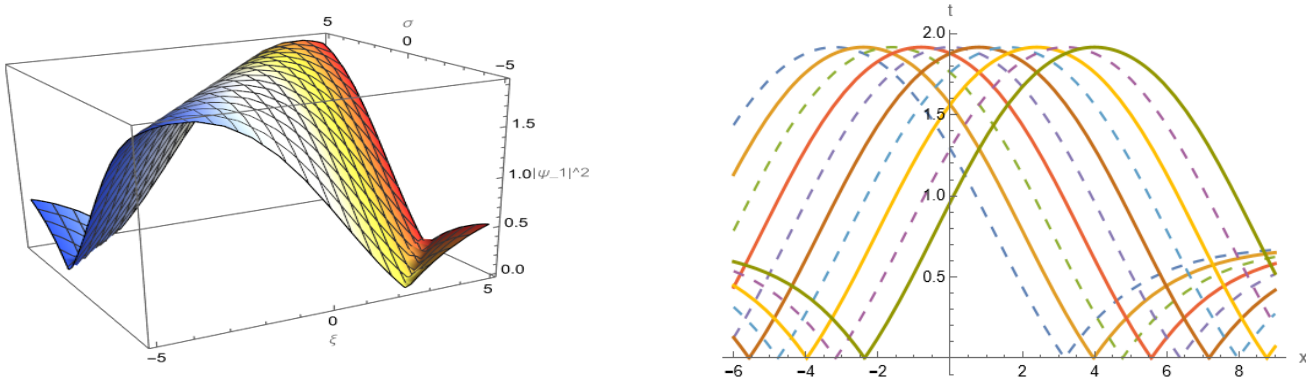

(a) **(b)**

Figure 25. Equation (4.8) represents a graphical behaviour of $\psi_1(x,t)$, if $\lambda_1 = 2.4$, $\lambda_2 = 3.7$, $\lambda_3 = 2.8$, $\lambda_4 = 0.19$, $\mu = 1.95$, $k_h = 0.3$, $k_c = 1.1$, $\tau = 0.52$, $V = 0.8$, $f = 0.8$, $\alpha = 1$, $\varphi_0 = 0$, $n_0 = 0.1$. (a) 3D graph, (b) 2D visual.

4.3. Two-fold HF-I

By containing the limit $\varrho \to 1$ in Eq (3.54), then the function transfer into

$$cn(\frac{\sqrt{\mp 2q\varrho_1(\Psi-\nu)}}{2\varrho\varrho_1}\sqrt{-\phi_3}(\varphi-\varphi_0),\varrho) \to sech(\frac{\sqrt{\mp 2q\varrho_1(\Psi-\nu)}}{2\varrho\varrho_1}\sqrt{-\phi_3}(\varphi-\varphi_0)),$$

which show the SW solution [39], see Figure 26.

$$\psi_1(\xi,\sigma) = \frac{vsech(\frac{\sqrt{\mp 2q\varrho_1(\Psi-\nu)}}{2\varrho\varrho_1}\sqrt{-\phi_3}(\varphi-\varphi_0)) + o}{ksech(\frac{\sqrt{\mp 2q\varrho_1(\Psi-\nu)}}{2\varrho\varrho_1}\sqrt{-\phi_3}(\varphi-\varphi_0)) + h} + \frac{\phi_2}{4}. \tag{4.9}$$

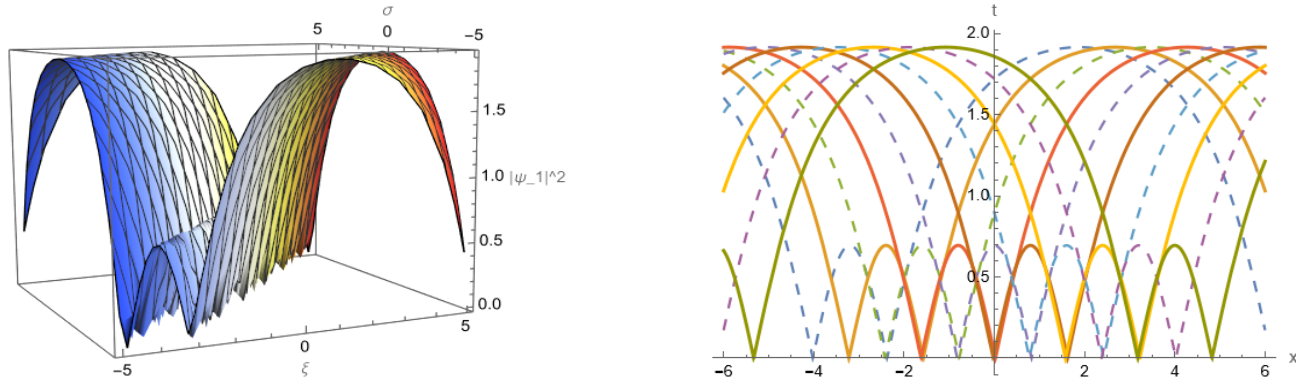

(a) **(b)**

Figure 26. Equation (4.9) an optical behaviour of $\psi_1(x,t)$, when $\lambda_1 = 3.4$, $\lambda_2 = 2.7$, $\lambda_3 = 2.8$, $\lambda_4 = 0.19$, $\mu = 1.95$, $k_h = 0.3$, $k_c = 1.1$, $\tau = 0.52$, $V = 0.8$, $f = 0.8$, $\alpha = 1$, $\varphi_0 = 0$, $n_0 = 0.1$. (a) 3D visualisation, (b) 2D plot.

4.4. *Two-fold PSW-II*

By containing the limit $\varrho \to 0$ in Eq (3.54), then the function transfer into

$$cn(\frac{\sqrt{\mp 2q\varrho_1(\Psi-\nu)}}{2\varrho\varrho_1}\sqrt{-\phi_3}(\varphi-\varphi_0),\varrho) \to \cos(\frac{\sqrt{\mp 2q\varrho_1(\Psi-\nu)}}{2\varrho\varrho_1}\sqrt{-\phi_3}(\varphi-\varphi_0)),$$

which show the SW solution [39], see Figure 27.

$$\psi_1(\xi,\sigma) = \frac{v\cos(\frac{\sqrt{\mp 2q\varrho_1(\Psi-\nu)}}{2\varrho\varrho_1}\sqrt{-\phi_3}(\varphi-\varphi_0)) + o}{k\cos(\frac{\sqrt{\mp 2q\varrho_1(\Psi-\nu)}}{2\varrho\varrho_1}\sqrt{-\phi_3}(\varphi-\varphi_0)) + h} + \frac{\phi_2}{4}. \tag{4.10}$$

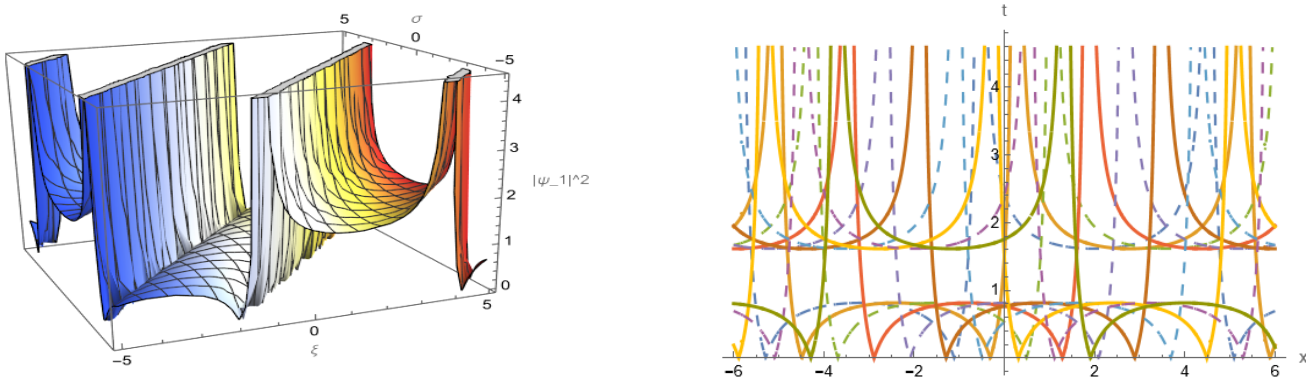

(a) **(b)**

Figure 27. Equation (4.10) construct a graphic of $\psi_1(x,t)$ under the following scenarios: $\Psi = 2.5$, $\nu = 1.7$, $\Theta = 2.87$, $q = 3.2$, $\mu = 1.95$, $k_h = 0.3$, $k_c = 1.1$, $\tau = 0.52$, $V = 0.8$, $f = 0.8$, $\alpha = 1$, $\varphi_0 = 0$, $n_0 = 0.1$. (a) 3D graph, (b) 2D display.

4.5. *Two-fold HF-III*

When $\varrho \to 1$ is utilized as the limit in Eq (3.58), then the functions turns into

$$sn(\eta\sqrt{-\phi_3}(\varphi-\varphi_0),\varrho) \to \tanh(\eta\sqrt{-\phi_3}(\varphi-\varphi_0)),$$

and

$$cn(\eta\sqrt{-\phi_3}(\varphi-\varphi_0),\varrho)\to sech(\eta\sqrt{-\phi_3}(\varphi-\varphi_0)),$$

which show the SW solution [39], see Figure 28.

$$\psi_1(\xi,\sigma)=\frac{c\tanh(\eta\sqrt{-\phi_3}(\varphi-\varphi_0))+esech(\eta\sqrt{-\phi_3}(\varphi-\varphi_0))}{h\tanh(\eta\sqrt{N}(\varphi-\varphi_0))+ksech(\eta\sqrt{-\phi_3}(\varphi-\varphi_0))}+\frac{\phi_2}{4}, \tag{4.11}$$

where $\eta=\frac{w_2\sqrt{(h^2+k^2)(\delta_1^2h^2+k^2)}}{h^2+k^2}$.

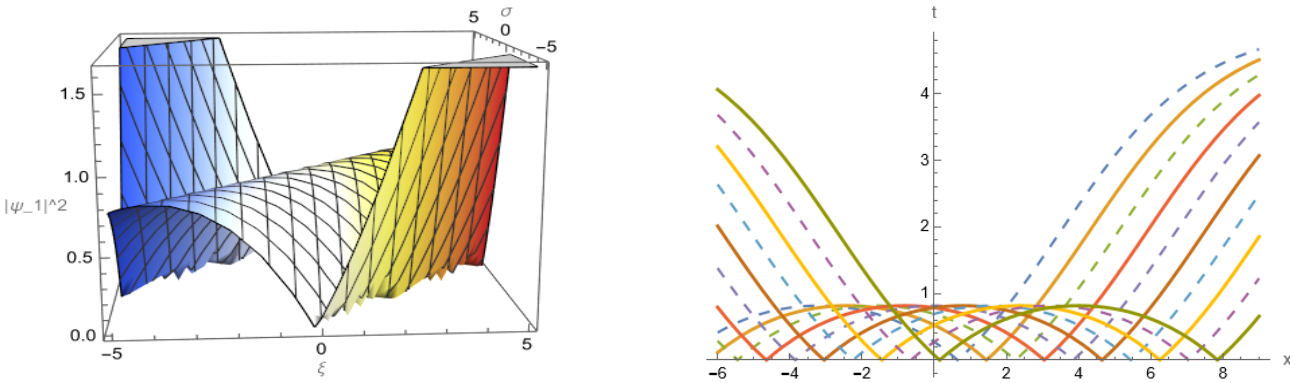

(a) **(b)**

Figure 28. Equation (4.11) demonstrates $\psi_1(x,t)$ graphically with values: $\psi=2.5$, $\nu=1.7$, $\Theta=1.87$, $q=2.2$, $\mu=1.95$, $k_h=0.3$, $k_c=1.1$, $\tau=0.52$, $V=0.8$, $f=0.8$, $\alpha=1$, $\varphi_0=0$, $n_0=0.1$. (a) 3D plot, (b) 2D visual.

4.6. Two-fold PSW-III

If $\varrho\to 0$ is the limit in Eq (3.58), the function yields

$$sn(\eta\sqrt{-\phi_3}(\varphi-\varphi_0),\varrho)\to\tanh(\eta\sqrt{-\phi_3}(\varphi-\varphi_0)),$$

and

$$cn(\eta\sqrt{-\phi_3}(\varphi-\varphi_0),\varrho)\to sech(\eta\sqrt{-\phi_3}(\varphi-\varphi_0)),$$

which show the SW solution [39], see Figures 29 and 30.

$$\epsilon(x,t)=\frac{c\tanh(\eta\sqrt{-\phi_3}(\varphi-\varphi_0))+esech(\eta\sqrt{-\phi_3}(\varphi-\varphi_0))}{h\tanh(\eta\sqrt{-\phi_3}(\varphi-\varphi_0))+ksech(\eta\sqrt{-\phi_3}(\varphi-\varphi_0))}+\frac{\phi_2}{4}, \tag{4.12}$$

where $\eta=\frac{w_2\sqrt{(h^2+k^2)(\delta_1^2h^2+k^2)}}{h^2+k^2}$.

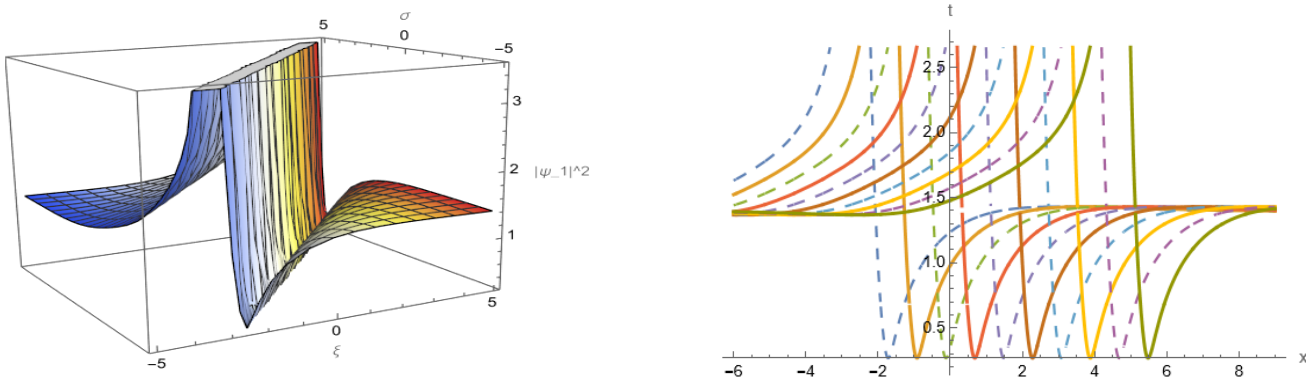

(a) **(b)**

Figure 29. Equation (4.11) illustrates $\psi_1(x,t)$ via visuals with values: $r_1 = 2.5$, $r_2 = 1.7$, $w_1 = 0.87$, $w_2 = 1.2$, $\mu = 1.95$, $k_h = 0.3$, $k_c = 1.1$, $\tau = 0.52$, $V = 0.8$, $f = 0.8$, $\alpha = 1$, $\varphi_0 = 0$, $n_0 = 0.1$. (a) 3D display, (b) 2D graph.

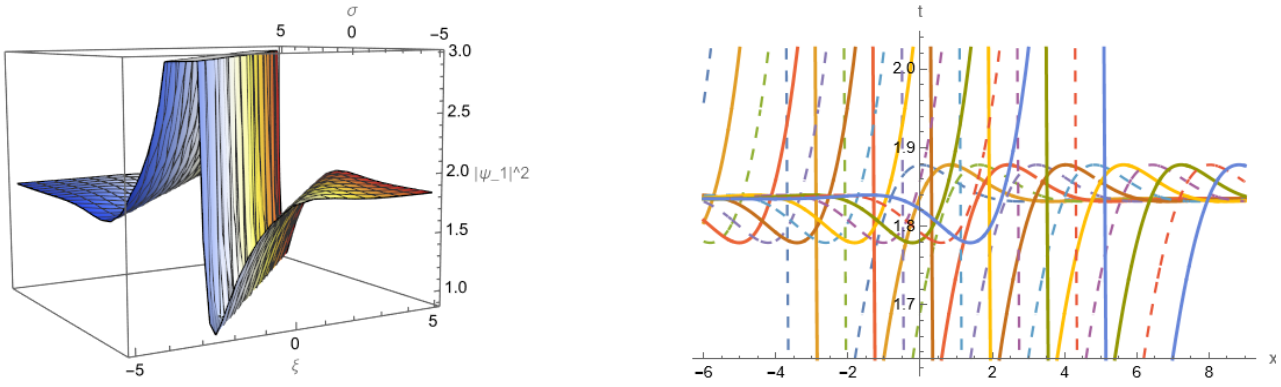

(a) **(b)**

Figure 30. Equation (4.12) displays $\psi_1(x,t)$ through visuals with values $r_1 = 2.5$, $r_2 = 1.7$, $w_1 = 0.87$, $w_2 = 1.2$, $\mu = 1.95$, $k_h = 0.3$, $k_c = 1.1$, $\tau = 0.52$, $V = 0.8$, $f = 0.8$, $\alpha = 1$, $\varphi_0 = 0$, $n_0 = 0.1$. (a) 3D image, (b) 2D representation.

5. CB

We introduce a perturbed term to investigate the possibility of chaotic behavior in the resultant system (1.12) [28]:

$$\begin{cases} L' = P(\varphi), \\ P' = -\phi_3(4L^3 + 2f_2L + f_1) + \chi_0 \cos(\omega\varphi), \end{cases} \tag{5.1}$$

where $\phi_3 = \frac{M}{2}$, $f_2 = \frac{-7\phi_2^2+16\phi_1}{16}$, $f_1 = \frac{\phi_2(\phi_2-4\phi_1)}{8}$, and $f_0 = \frac{-2\phi_2^4+64\phi_2^2\phi_1+256\phi_0}{256}$.

Now, Eq (5.1) ω is the frequency and χ_0 is the disruption of strength. System (5.1) possesses an external periodic force that system (22) lacks, enabling one to study the periodicity and chaotic patterns of Eq (1.1). To solve this problem, we employ various tools such as time series profiling, phase portrait method and Poincare maps. We will consider two alternate scenarios and study the influence of the

various parameters ϕ_3, f_2, f_0, χ_0, and ω in order to study the matter from different points of view. Under the first scenario, χ_0 and ω are constants, and we will study the influence of changing the other factors. While under the second scenario, we'll study the influence of χ_0 with constant values of ϕ_3, f_2, f_0, ω. Figure 31 is showing time analysis graphs, Poincare maps, 3D and 2D graphs with respect to $\phi_3 = 1.375$, $f_2 = 1.27$, $f_1 = -0.72$, $\chi_0 = 3.5$, and $\omega = 2\pi$. System (86), for $\chi_0 = 3.5$, is exhibited to display quasi-periodic behavior. We take $\phi_3 = 0.62$, $f_2 = 3.63$, and $f_1 = -1.24$ with $\chi_0 = 3.5$ in Figure 32. We have $\phi_3 = 0.5$, $f_2 = 1.5$, and $f_1 = -1.6$ with $\chi_0 = 2.5$ in Figure 33. System (5.1) is found to be quasi-periodic in nature but, for specified values of parameters, the Poincare section contains several disordered points indicating chaotic behavior. We only vary χ_0 in Figure 33 from Figure 34 with $\chi_0 = 1.5$. Rest all components remain constant. System (86) is quasi-periodic in nature compared to chaotic activity exhibited by the Poincare map, which contains many irregular regions.

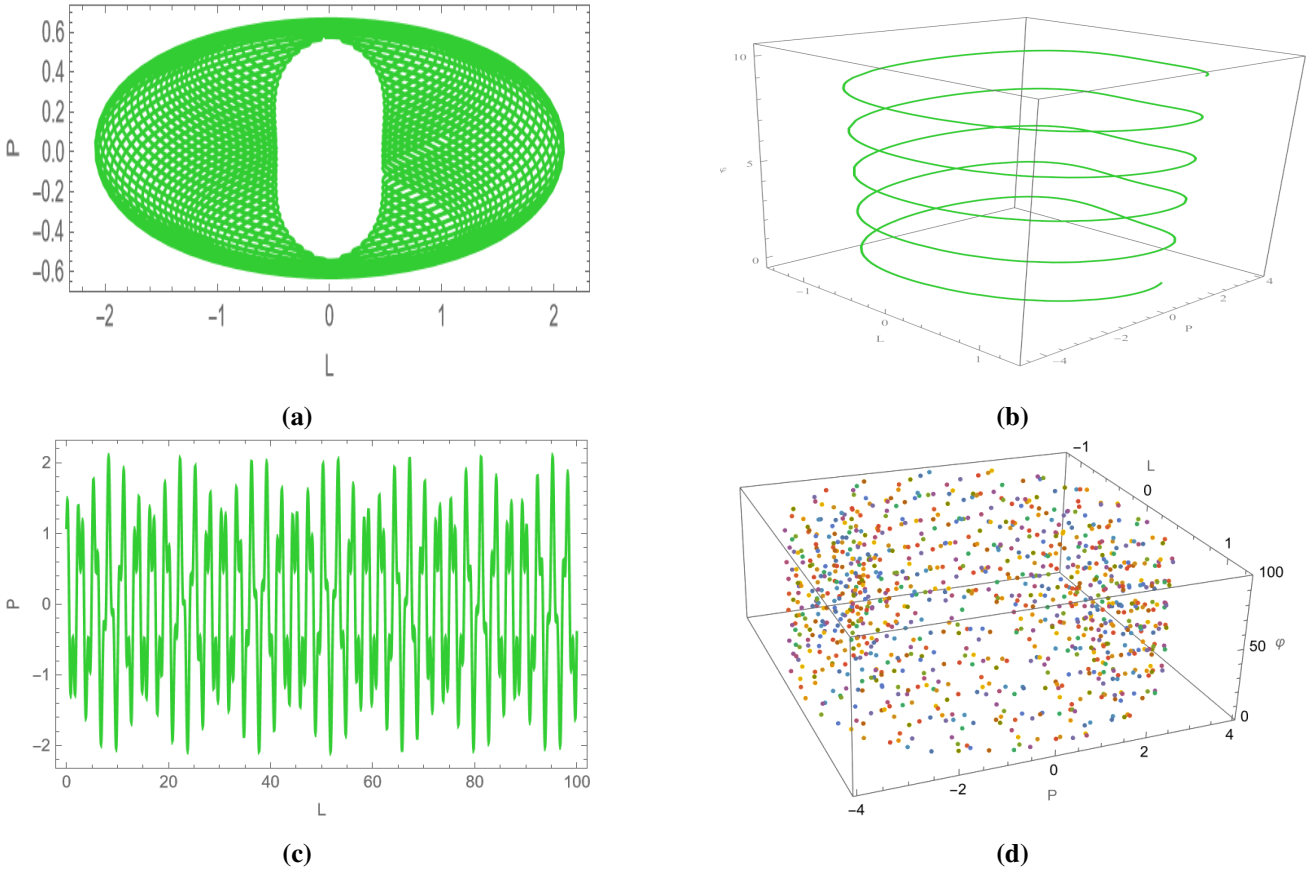

Figure 31. CB for Eq (5.1) with initial conditions $(0.08, 0.08)$ and parameters $\phi_3 = 1.375$, $f_2 = 1.27$, $f_1 = -0.72$, $\chi_0 = 3.5$, and $\omega = 2\pi$. (a) Phase plane image, (b) 3D helical graph, (c) time series plot, (d) 3D scatter visual.

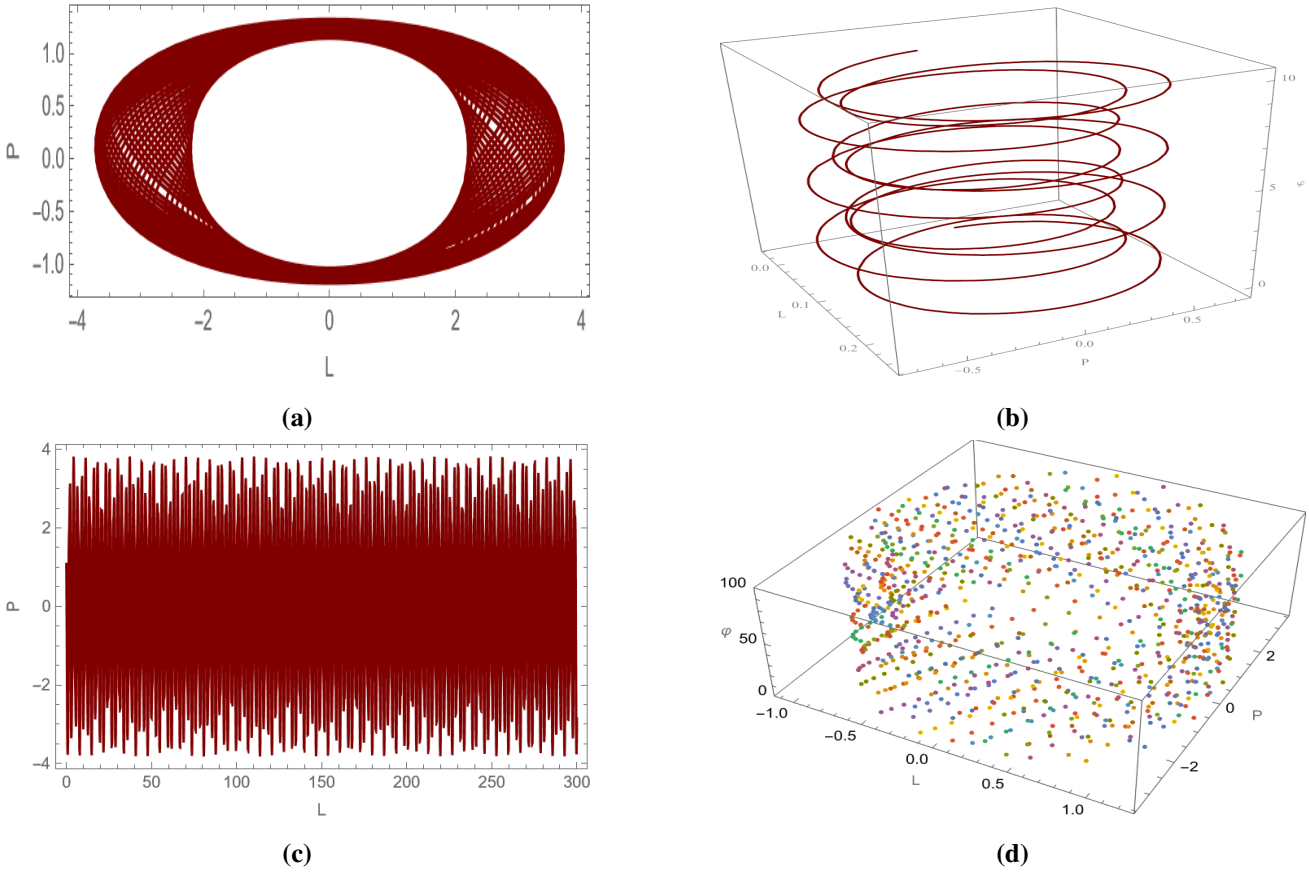

Figure 32. CB with initial condition (1.08, 1.08) and parameters values $\phi_3 = 0.62$, $f_2 = 3.63$, $f_1 = -1.24$, $\chi_0 = 3.5$, and $\omega = 2\pi$. (a) Phase plane image, (b) 3D helical plot, (c) time series image, (d) 3D scatter display.

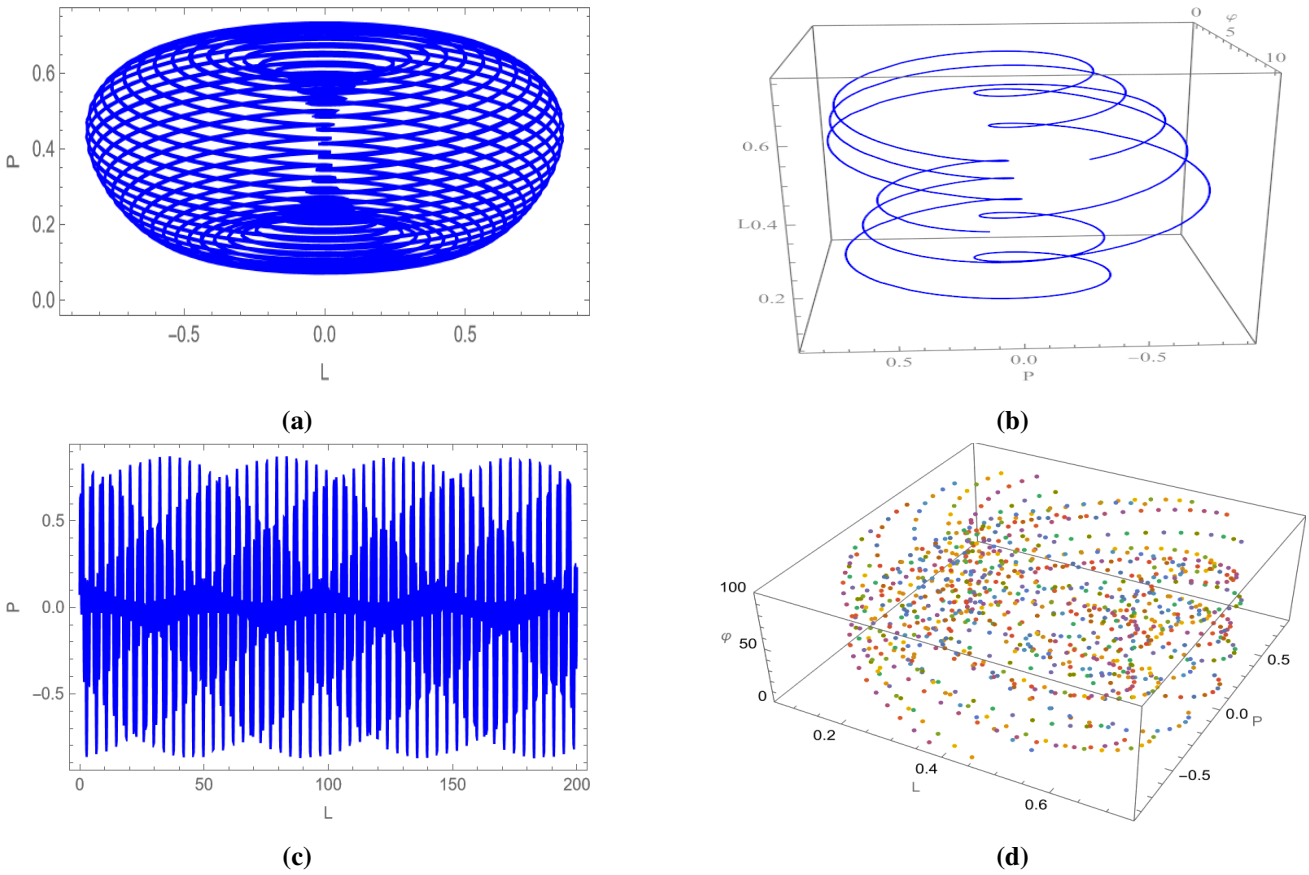

Figure 33. CB with $(0.08, 0.08)$ and parameters $\phi_3 = 0.5$, $f_2 = 1.5$, $f_1 = -1.6$, $\chi_0 = 2.5$, and $\omega = 2\pi$. (a) Phase plane graph, (b) 3D helical visual, (c) time series plot, (d) 3D scatter projection.

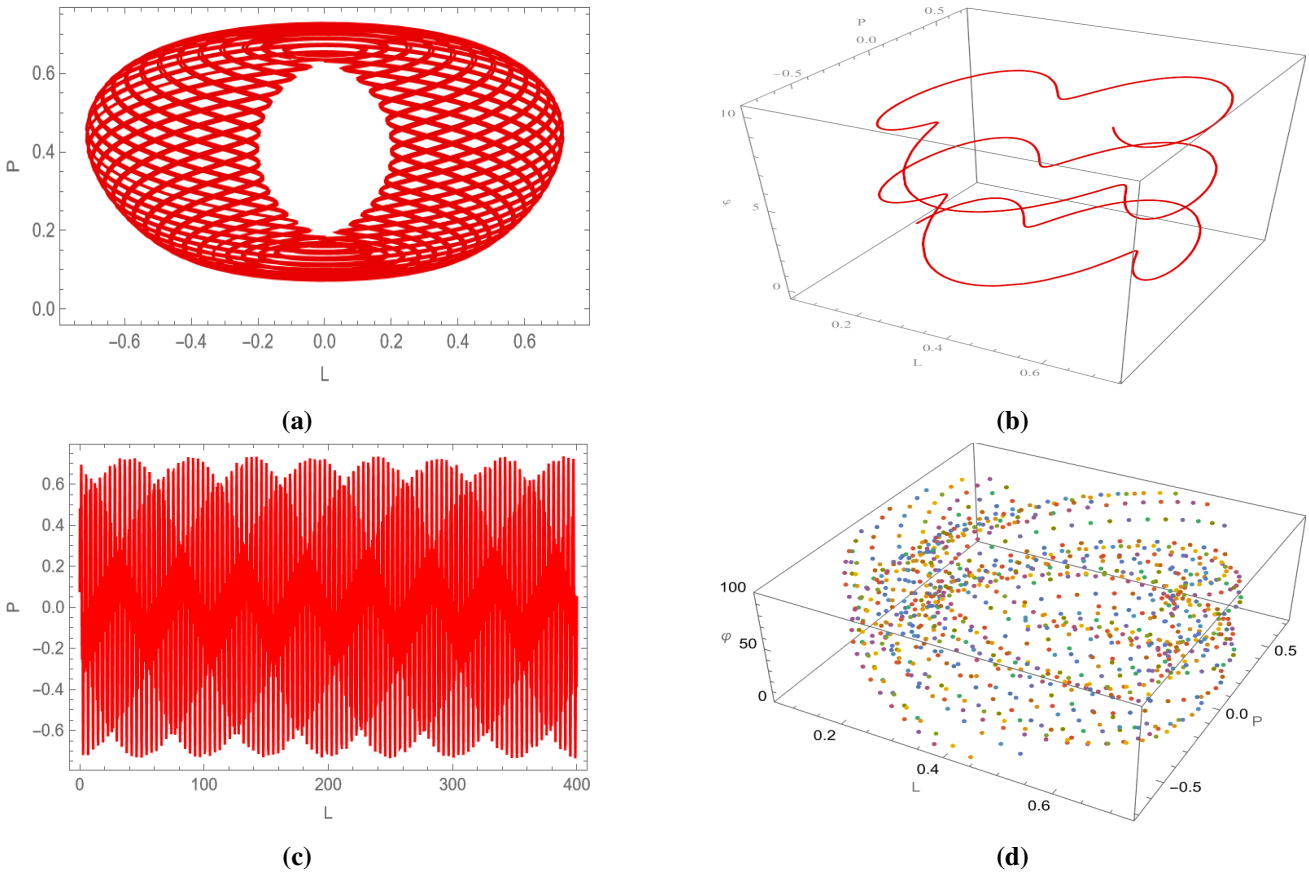

Figure 34. CB for Eq (5.1) with $(0.08, 0.08)$ and parameters $\phi_3 = 0.5$, $f_2 = 1.5$, $f_1 = -1.6$, $\chi_0 = 1.5$, and $\omega = 2\pi$. (a) Phase plane illustration, (b) 3D helical diagram, (c) time series graph, (d) 3D scatter plot.

6. The energy balance method

Here, we applying the energy balance equation. To do so, we rewrite the Eq (3.3) as:

$$\frac{\psi_1'^2}{2} + \frac{M}{4}\psi_1^4 + \frac{N}{3}\psi_1^3 + \frac{Q}{2}\psi_1^2 = 0. \tag{6.1}$$

It's variation principle is as follows:

$$K(\psi_1) = \int_0^{\frac{\tau}{4}} \left(\frac{\psi_1'^2}{2} - (-\frac{M}{4}\psi_1^4 - \frac{N}{3}\psi_1^3 - \frac{Q}{2}\psi_1^2) d\varphi \right) \tag{6.2}$$

$$K(\psi_1) = \int_0^{\frac{\tau}{4}} (C - W) d\varphi. \tag{6.3}$$

Here, V is the kinetic energy and W is potential energy, so,

$$C = \frac{\psi_1'^2}{2}, \quad W = -\frac{M}{4}\psi_1^4 - \frac{N}{3}\psi_1^3 - \frac{Q}{2}\psi_1^2. \tag{6.4}$$

Its Hamiltonian invariant is as follows:

$$H = C + W = (\frac{\psi_1'^2}{2} + (-\frac{M}{4}\psi_1^4 - \frac{N}{3}\psi_1^3 - \frac{Q}{2}\psi_1^2). \tag{6.5}$$

Now, we assume the solution of Eq (5.2) is:

$$\psi_1(\varphi) = \zeta \cos(\varrho\varphi). \tag{6.6}$$

According to energy balance method, Hamiltonian invariant needs to be unchanged:

$$H = C + W = (\frac{\psi_1'^2}{2} + (-\frac{M}{4}\psi_1^4 - \frac{N}{3}\psi_1^3 - \frac{Q}{2}\psi_1^2) = H_0. \tag{6.7}$$

The initial condition of Eq (6.6) is:

$$\psi_1(0) = 0, \psi_1(0) = \zeta. \tag{6.8}$$

Putting Eq (6.8) into Eq (6.7):

$$-\frac{M}{4}\zeta^4 - \frac{N}{3}\zeta^3 - \frac{Q}{2}\zeta^2 = H_0. \tag{6.9}$$

Next, putting Eqs (6.9) and (6.7) into Eq (6.8), we get:

$$\frac{(\zeta\varrho\sin(\varrho\varphi))^2}{2} - \left(\frac{M}{4}(\zeta\cos(\varrho\varphi))^4 + \frac{N}{3}(\zeta\cos(\varrho\varphi))^3 + \frac{Q}{2}(\zeta\cos(\varrho\varphi))^2\right) = -\frac{M}{4}\zeta^4 - \frac{N}{3}\zeta^3 - \frac{Q}{2}\zeta^2), \tag{6.10}$$

On substituting $\varrho\varphi = \frac{\pi}{4}$ into Eq (6.11), we get:

$$\frac{\zeta^2\varrho^2}{4} - \zeta^4\frac{M}{16} - \zeta^3\frac{N}{6\sqrt{2}} - \zeta^2\frac{Q}{4} = -\frac{M}{4}\zeta^4 - \frac{N}{3}\zeta^3 - \frac{Q}{2}\zeta^2. \tag{6.11}$$

Hence, we have:

$$\varrho = \sqrt{\frac{-3M}{4}\zeta^2 + N(\frac{-4+\sqrt{2}}{3})\zeta - Q}. \tag{6.12}$$

So, we get the periodic solution of Eq (3.3), see Figures 35 and 36.

$$\psi_1(\varphi) = \left(\zeta\cos\left(\sqrt{\frac{-3M}{4}\zeta^2 + N(\frac{-4+\sqrt{2}}{3})\zeta - Q}\right)\varphi\right), \tag{6.13}$$

where $\varphi = (\frac{1}{\alpha})\xi^\alpha - V(\frac{1}{\alpha})\sigma^\alpha$.

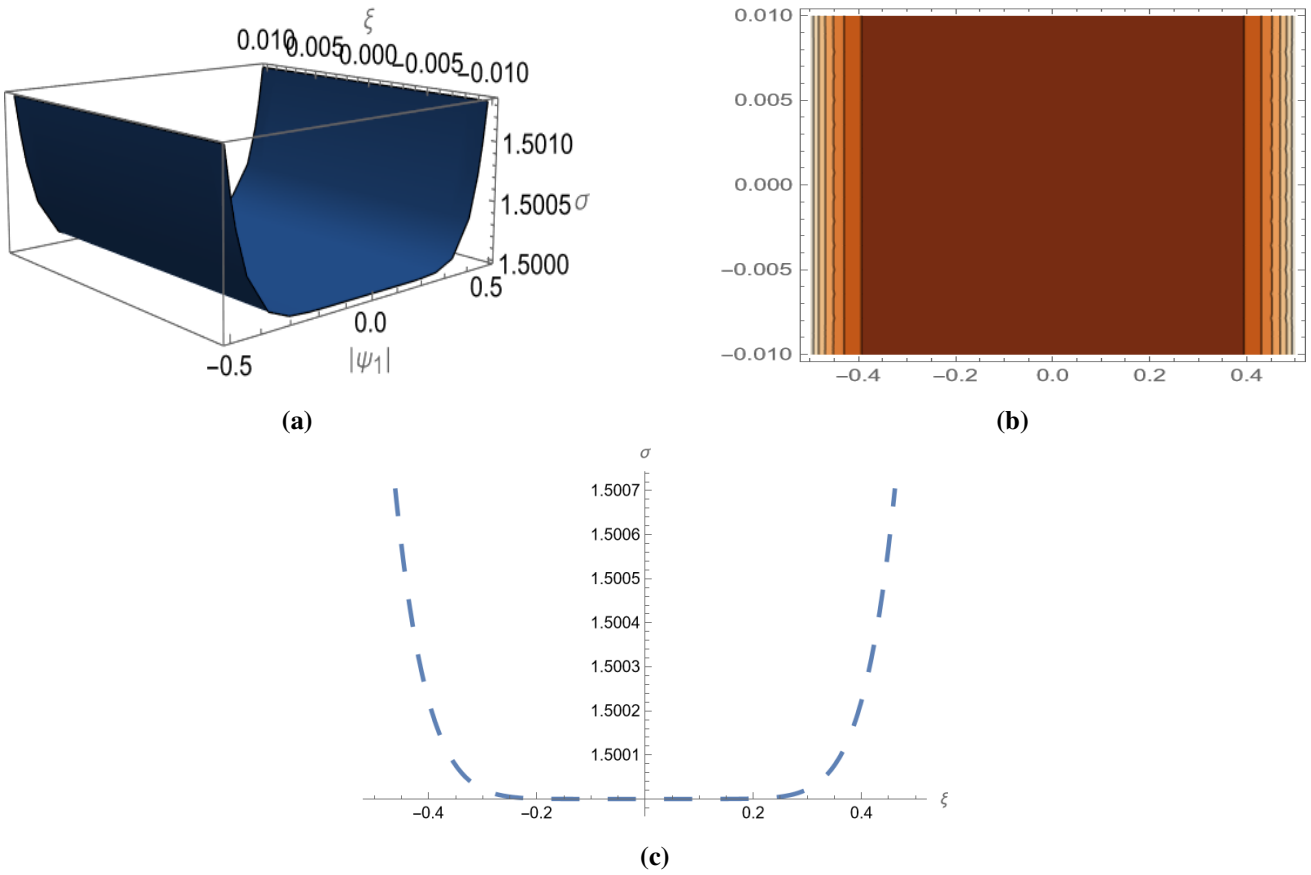

(a) **(b)**

(c)

Figure 35. Equation (6.13) recognizes the graphic form of $\psi_1 = (\xi, \sigma)$ by using following values $M = -3$, $N = 7$, $Q = 3.3$, $V = 7$, $\zeta = 1.5$, $\alpha = 4$. (a) 3D plot, (b) contour graph, (c) 2D diagram.

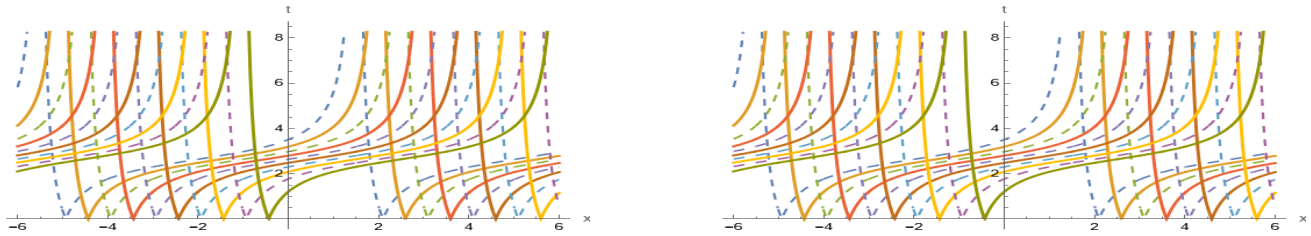

(a) 3D image **(b)** 2D representation

Figure 36. Equation (85) displays $\psi_1(x,t)$ through visuals with values $r_1 = 2.5$, $r_2 = 1.7$, $w_1 = 0.87$, $w_2 = 1.2$, $\mu = 1.95$, $k_h = 0.3$, $k_c = 1.1$, $\tau = 0.52$, $V = 0.8$, $f = 0.8$, $\alpha = 1$, $\varphi_0 = 0$, $n_0 = 0.1$. (a) 3D image, (b) 2D representation.

7. Results and discussion

Here, we discuss our findings and make comparisons with earlier findings. Eslami analyzed extended KdV for finding new analytical solutions by using exponential method [23]. Using definitions of fractional derivatives, they sought to obtain new analytical solutions of the KdV equation using

the exponential method and were able to establish a new class of solutions with graphical analysis. Neirameh and Eslami analyzed EKdVE for finding analytical and exact solutions by means of Riccati equation method [21]. They aimed to obtain new exact analytical solutions for the EKdVE equation by employing a new modified method called the Riccati equation method. EKdV equation was presented through the reductive perturbation method, with a double-layer structure being incorporated within the existing plasma model. Their resulting solutions were given by means of hyperbolic, trigonometric, and rational functions. Neirameh and Memarian analyzed extended KdV for finding new exact SW solutions by means of an analytical method [22]. They examined the double-layer structure model of the EKdVE according to the reductive perturbation method, which added a double-layer structure to the current plasma model. Applying the (G'/G)-expansion method, they derived new exact solitary wave solutions to the equation successfully. Two parallel sheets of opposite electric charges constitute a double layer of plasma, generating a strong electric field with a sharp difference in potentials within the two layers. Such a structure is thought to feature prominently in a myriad of space plasma environments around Earth as well as in a number of astrophysical objects. These nonlinear entities naturally exist within a vast array of space plasma conditions and are typically addressed by the KdV equation with the addition of cubic nonlinearity to describe different homogeneous plasma regimes.

In this paper, we have used the CDSP approach which provides considerable benefits for the solution of nonlinear evolution equations. It provides a unified, systematic approach that removes the necessity for spurious assumptions regarding the shape of solutions. Analyzing the complete discriminant structure of the corresponding polynomial naturally classifies and generates a broad range of exact solutions, such as hyperbolic, trigonometric, rational, and Jacobi elliptic function ones, see Table 2.

Table 2. Appendix.

Variables	Physical meaning
T_c, T_h	Temperature of cold and hot electrons, respectively
κ_c, κ_h	Spectral index measuring deviations from Maxwell equilibrium for cold and hot electrons
n_c, n_h	Density of cold and hot electrons, respectively
$\Phi(x,t)$	Wave profile depending on spatial and temporal coordinates
sn, cn	Jacobi elliptic functions
V, W	Kinetic and potential energy
H	Hamiltonian invariant

This exhaustive classification prevents the exclusion of any possible solution type. Additionally, CDSPM is extremely effective for solving high-order nonlinear equations, where other methods are bound to fail. Apart from finding explicit solutions, it also assists in qualitative understanding of the system dynamics, such as stability analysis, bifurcation behavior, and chaotic features. Compared with conventional ansatz-based or residual-balancing methods, CDSPM is more stable, flexible, and rooted deep within the inherent mathematics of the governing equations, hence a better analytical tool for investigating intricate nonlinear phenomena. We have discussed several types of soliton solutions, where triangular function periodic solutions from Eq (35) are shown in Figure 5. Periodic solutions, which repeat their action within a standard interval of time, have a significant role for all branches of science, science, as well as various branches of science. Equations (3.32), (3.33), (3.41), (3.62), and

(3.63) show SW solutions are plotted from Figures 7, 8, 11, 18, and 19. SW solutions are helpful for all branches of science such as, nonlinear optics, physics, biology, plasma physics due to one of their common characteristics. From Eqs (3.28), (3.36), and (3.38), rational soliton solutions shown from Figures 6, 9, and 10. From Eqs (3.45), (3.46), (3.49), and (3.50), JEF double periodic solutions graphical behavior are shown from Figures 12–15, if we take the limits as $\varrho \to 1$ and $\varrho \to 0$,then the solutions are double hyperbolic-I SW from Eqs (4.1)–(4.4) and their characteristics are from Figures 19–22, and double periodic-I SW from Eqs (4.5)–(4.8) are shown from Figures 23–26. From Eq (3.54), JEF double periodic solutions as well as their graphical behavior are shown from Figure 16, but if we take the limits as $\varrho \to 1$ as well as $\varrho \to 0$ to become double hyperbolic-II SW from Eq (4.9) as well as double periodic-II from Eq (4.10), their graphs are shown from Figures 27 as well as 28. From Eq (3.58), we have JEF double periodic solution as well as their shape of profile show from Figure 17, but if we take the limits as $\varrho \to 1$ as well as $\varrho \to 0$, then, it becomes double hyperbolic-III from Eq (4.11) as well as double periodic-III from Eq (4.12) as well as their graphical representation from Figure 29 as well as 30. And, we apply energy balance method from Eq (6.13) to get the periodic behavior, which is shown from Figure 31. They assist us with a more effective understanding of the dynamics of systems as well as their reaction to various parameters. Various of these solutions provide valuable insights into the contribution of wave phenomena to physical systems. They are applied in telecommunications, plasma physics, and quantum mechanics. Additionally, we perform a bifurcation as well as a chaos. These analyses are utilized in various applications of science and technology to understand underlying dynamics, control systems, as well as predict.

8. Conclusions

In the present work, we have examined the EKdVE model of fractional derivatives using the CDSPM. With this method, we were able to derive diverse soliton and solitary-wave patterns, such as rational solutions, Jacobi elliptic function (JEF) double periodic waves, solitary waves, periodic waves, and transformation of JEF double periodic waves into solitary waves. We also examined the model's bifurcation structure as well as its chaotic dynamics to perform a qualitative investigation. Our model was reduced to a planar dynamical system using a Galilean transform, which facilitated a thorough examination of its stability. Our quasi-periodic as well as chaotic dynamics were subsequently studied by incorporating a source of external periodic driving. For the detection as well as identification of chaos, we employed several methods, including 2D and 3D graphical results, time series plots, as well as Poincare maps. All results from the above conclusively prove the efficacy, flexibility, as well as extensive applicability of the methods proposed for studying soliton dynamics as well as phase transitions of nonlinear models. Additionally, the research utilized the energy balance method, which gained huge importance due to its efficacy for resolving NLPDEs. Utilization of CDSPM provides considerable benefits, such as a systematic unified framework for the classification of all possible types of solutions, avoidance of arbitrariness of assumptions, and improvement of analytical tractability of higher-order nonlinear equations. Its power for naturally solving a vast range of exact forms of the solution as well as gaining insights into the qualitative dynamics makes the CDSPM a very effective as well as a reliable method for investigating complex nonlinear evolution equations.

Use of Generative-AI tools declaration

The authors declare they have not used Artificial Intelligence (AI) tools in the creation of this article

Author contributions

Syed T. R. Rizvi: Methodology, formal analysis, conceptualization, writing-original draft preparation; M. A. Abdelkawy: Validation, visualization, reviewing; Hanadi Zahed: Resources, investigation, reviewing; Aly R. Seadawy: Supervision, methodology, software; All authors have read and approved the final version of the manuscript for publication.

Acknowledgements

This work was supported and funded by the Deanship of Scientific Research at Imam Mohammad Ibn Saud Islamic University (IMSIU) (grant number IMSIU-DDRSP2502).

Conflicts of interest

The authors declare they have no conflict of interest.

References

1. N. Vassena, F. Avram, R. Adenane, Finding bifurcations in mathematical epidemiology via reaction network methods, *Chaos*, **34** (2024), 123163. https://doi.org/10.1063/5.0221082
2. J. B. Li, Y. Q. Yang, W. Y. Sun, Breather wave solutions on the Weierstrass elliptic periodic background for the (2+1)-dimensional generalized variable-coefficient KdV equation, *Chaos*, **34** (2024), 023141. https://doi.org/10.1063/5.0192185
3. Y.-H. Huang, R. Guo, Wave breaking, dispersive shock wave, and phase shift for the defocusing complex modified KdV equation, *Chaos*, **34** (2024), 103103. https://doi.org/10.1063/5.0231741
4. Z. J. Lin, Z. Y. Yan, Interactions and asymptotic analysis of N-soliton solutions for the n-component generalized higher-order Sasa-Satsuma equations, *Chaos*, **34** (2024), 123145. https://doi.org/10.1063/5.0237425
5. L. L. Zhang, H. T. Han, N-Soliton solutions of coupled Schrödinger-Boussinesq equation with variable coefficients, *Commun. Nonlinear Sci.*, **138** (2024), 108185. https://doi.org/10.1016/j.cnsns.2024.108185
6. Y. G. Kao, C. H. Wang, H. W. Xia, Y. Cao, Projective synchronization for uncertain fractional reaction-diffusion systems via adaptive sliding mode control based on finite-time scheme, In: *Analysis and control for fractional-order systems*, Singapore: Springer, 2024, 141–163. https://doi.org/10.1007/978-981-99-6054-5_8
7. F. Y. Liu, Y. Q. Yang, Q. Chang, Synchronization of fractional-order delayed neural networks with reaction–diffusion terms: distributed delayed impulsive control, *Commun. Nonlinear Sci.*, **124** (2023), 107303. https://doi.org/10.1016/j.cnsns.2023.107303

8. X. Meng, Y. G. Kao, H. R. Karimi, C. C. Gao, Global Mittag-Leffler stability for fractional-order coupled systems on network without strong connectedness, *Sci. China Inf. Sci.* , **63** (2020), 132201. https://doi.org/10.1007/s11432-019-9946-6
9. Y. Cao, Y. G. Kao, Z. Wang, X. S. Yang, J. H. Park, W. Xie, Sliding mode control for uncertain fractional-order reaction–diffusion memristor neural networks with time delays, *Neural Networks*, **178** (2024), 106402. https://doi.org/10.1016/j.neunet.2024.106402
10. Y. G. Kao, C. H. Wang, H. W. Xia, Y. Cao, Global Mittag-Leffler synchronization of coupled delayed fractional reaction-diffusion Cohen-Grossberg neural networks via sliding mode control, In: *Analysis and control for fractional-order systems*, Singapore: Springer, 2024, 121–140. https://doi.org/10.1007/978-981-99-6054-5_7
11. A. Ali, A. R. Seadawy, D. C. Lu, New solitary wave solutions of some nonlinear models and their applications, *Adv. Differ. Equ.*, **2018** (2018), 232. https://doi.org/10.1186/s13662-018-1687-7
12. M. S. Ullah, M. Z. Ali, H.-O. Roshid. Stability analysis, ϕ^6 model expansion method, and diverse chaos-detecting tools for the DSKP model, *Sci. Rep.*, **15** (2025), 13658. https://doi.org/10.1038/s41598-025-98275-7
13. A. R. Seadawy, D. C. Lu, C. Yue, Travelling wave solutions of the generalized nonlinear fifth-orderKdV water wave equations and its stability, *J. Taibah Univ. Sci.*, **11** (2017), 623–633. https://doi.org/10.1016/j.jtusci.2016.06.002
14. M. Arshad, A. R. Seadawy, D. C. Lu, Elliptic function and solitary wave solutions of the higher-order nonlinear Schrödinger dynamical equation with fourth-order dispersion and cubic-quintic nonlinearity and its stability, *Eur. Phys. J. Plus*, **132** (2017), 371. https://doi.org/10.1140/epjp/i2017-11655-9
15. A. H. Khater, D. K. Callebaut, W. Malfliet, A. R. Seadawy, Nonlinear dispersive Rayleigh-Taylor instabilities in magnetohydrodynamic flows, *Phys. Scr.*, **64** (2001), 533. https://doi.org/10.1238/Physica.Regular.064a00533
16. L. Akinyemi, A. Houwe, S. Abbagari, A.-M. Wazwaz, H. M. Alshehri, M. S. Osman, Effects of the higher-order dispersion on solitary waves and modulation instability in a monomode fiber, *Optik*, **288** (2023), 171202. https://doi.org/10.1016/j.ijleo.2023.171202
17. F. Badshah, K. U. Tariq, M. Inc, M. Aslam, M. Zeeshan, On the study of bright, dark and optical wave structures for the coupled fractional nonlinear Schrödinger equations in plasma physics, *Opt. Quant. Electron.*, **55** (2023), 1170. https://doi.org/10.1007/s11082-023-05434-z
18. M. Inc, R. T. Alqahtani, M. S. Iqbal, Statblity analysis and consistent solitary wave solutions for the reaction diffusion regularised nonlinear model, *Results Phys.*, **54** (2023), 107053. https://doi.org/10.1016/j.rinp.2023.107053
19. U. K. Manda, A. Das, W.-X. Ma, Integrability, breather, rogue wave, lump, lump-multi-stripe, and lump-multi-soliton solutions of a (3+1)-dimensional nonlinear evolution equation, *Phys. Fluids*, **36** (2024), 037151. https://doi.org/10.1063/5.0195378
20. A.-M. Wazwaz, W. Alhejaili, S. A. El-Tantawy, Study on extensions of (modified) Korteweg–de Vries equations: Painlevé integrability and multiple soliton solutions in fluid mediums, *Phys. Fluids*, **35** (2023), 093110. https://doi.org/10.1063/5.0169733

21. A. Neirameh, M. Eslami, New travelling wave solutions for plasma model of extended K-dV equation, *Afr. Mat.*, **30** (2019), 335–344. https://doi.org/10.1007/s13370-018-00651-2
22. A. Neirameh, N. Memarian, New analytical soliton type solutions for double layers structure model of extended KDV equation, *Computational Methods for Differential Equations*, **5** (2017), 256–270.
23. M. Eslami, Optical solutions to a conformable fractional extended KdV model equation, *Partial Differential Equations in Applied Mathematics*, **8** (2023), 100562. https://doi.org/10.1016/j.padiff.2023.100562
24. L.-C. Shi, Applications of complete discrimination system for polynomial for classifications of traveling wave solutions to nonlinear differential equations, *Comput. Phys. Commun.*, **181** (2010), 317–324. https://doi.org/10.1016/j.cpc.2009.10.006
25. T. Usman, I. Hossain, M. S. Ullah, M. M. Hasan, Soliton, multistability, and chaotic dynamics of the higher-order nonlinear Schrödinger equation, *Chaos*, **35** (2025), 043141. https://doi.org/10.1063/5.0266469
26. S. T. R. Rizvi, S. Shabbir, Optical soliton solution via complete discrimination system approach along with bifurcation and sensitivity analyses for the Gerjikov-Ivanov equation, *Optik*, **294** (2023), 171456. https://doi.org/10.1016/j.ijleo.2023.171456
27. Y. Kai, S. Q. Chen, B. L. Zheng, K. Zhang, N. Yang, W. L. Xu, Qualitative and quantitative analysis of nonlinear dynamics by the complete discrimination system for polynomial method, *Chaos Soliton. Fract.*, **141** (2020), 110314. https://doi.org/10.1016/j.chaos.2020.110314
28. S. S. Kazmi, A. Jhangeer, N. Raza, H. I. Alrebdi, A.-H. Abdel-Aty, H. Eleuch, The analysis of bifurcation, quasi-periodic and solitons patterns to the new form of the generalized q-deformed Sinh-Gordon equation, *Symmetry*, **15** (2023), 1324. https://doi.org/10.3390/sym15071324
29. S. Wael, E. A. Ahmed, A. R. Seadawy, R. S. Ibrahim, Bifurcation, similarity reduction, conservation laws and exact solutions of modified-Korteweg-de Vries–Burger equation, *Opt. Quant. Electron.*, **55** (2023), 262. https://doi.org/10.1007/s11082-022-04517-7
30. A. H. Tedjani, A. R. Seadawy, S. T. R. Rizvi, E. Solouma, Construction of Hamiltonina and optical solitons along with bifurcation analysis for the perturbed Chen–Lee–Liu equation, *Opt. Quant. Electron.*, **55** (2023), 1151. https://doi.org/10.1007/s11082-023-05403-6
31. A. R. Seadawy, A. Ahmad, S. T. R. Rizvi, S. Ahmed, Bifurcation solitons, Y-type, distinct lumps and generalized breather in the thermophoretic motion equation via graphene sheets, *Alex. Eng. J.*, **87** (2024), 374–388. https://doi.org/10.1016/j.aej.2023.12.023
32. S. T. R. Rizvi, A. R. Seadawy, S. K. Naqvi, M. Ismail, Bifurcation analysis for mixed derivative nonlinear Schrödinger's equation, helix nonlinear Schrödinger's equation and Zoomeron model, *Opt. Quant. Electron.*, **56** (2024), 452. https://doi.org/10.1007/s11082-023-06100-0
33. S. Kumar, H. Kharbanda, Chaotic behavior of predator-prey model with group defense and non-linear harvesting in prey, *Chaos Soliton. Fract.*, **119** (2019), 19–28. https://doi.org/10.1016/j.chaos.2018.12.011

34. H. Kharbanda, S. Kumar, Chaos detection and optimal control in a cannibalistic prey-predator system with harvesting, *Int. J. Bifurcat. Chaos*, **30** (2020), 2050171. https://doi.org/10.1142/S0218127420501710

35. S. Kumar, H. Kharbanda, Sensitivity and chaotic dynamics of an eco-epidemiological system with vaccination and migration in prey, *Braz. J. Phys.*, **51** (2021), 986–1006. https://doi.org/10.1007/s13538-021-00862-2

36. M. H. Rafiq, N. Raza, A. Jhangeer, Dynamic study of bifurcation, chaotic behavior and multi-soliton profiles for the system of shallow water wave equations with their stability, *Chaos Soliton. Fract.*, **171** (2023), 113436. https://doi.org/10.1016/j.chaos.2023.113436

37. Z. Li, C. Huang, Bifurcation, phase portrait, chaotic pattern and optical soliton solutions of the conformable Fokas-Lenells model in optical fibers, *Chaos Soliton. Fract.*, **169** (2023), 113237. https://doi.org/10.1016/j.chaos.2023.113237

38. X. Zhang, F. H. Min, Y. P. Dou, Y. Y. Xu, Bifurcation analysis of a modified FitzHugh-Nagumo neuron with electric field, *Chaos Soliton. Fract.*, **170** (2023), 113415. https://doi.org/10.1016/j.chaos.2023.113415

39. A. Filiz, M. Ekici, A. Sonmezoglu, F-Expansion method and new exact solutions of the Schrödinger-KdV equation, *Sci. World J.*, **2014** (2014), 534063. https://doi.org/10.1155/2014/534063

AIMS Press